DESIGN OF A FIBER OPTIC SENSOR ARRAY FOR IN VITRO MONITORING OF CELLULAR PROCESSES

Douglas Page West

Thesis submitted to the Faculty of the
Virginia Polytechnic Institute and State University
in partial fulfillment of the requirements for the degree of

Master of Science
in
Materials Science and Engineering

Dr. Richard O. Claus, Chair
Dr. Thomas Toth
Dr. Kent Murphy

February, 1998
Blacksburg, Virginia

Keywords: Fiber Optic Monitoring, Monitoring Cellular Processes

Copyright 1998, Douglas P. West

Design of a Fiber Optic Sensor Array for In Vitro Monitoring of Cellular Processes

by
Douglas Page West

Dr. Richard O. Claus, Chairman
Bradley Department of Electrical Engineering
Virginia Polytechnic Institute and State University

Abstract

Current analysis of the life and death cycles of in vitro cellular systems is based on visual observation methods relying upon morphological changes monitored using a microscope. Data collected from these techniques are not as precise as scientists desire them to be. The methods are discontinuous, indirect, costly, and time and labor intensive. The human element plays a significant part in error propagation as individual style of the researcher lends to skewing the data. Experimental results will differ greatly from laboratory to laboratory just because the methods of monitoring cellular activity are not standardized. The researcher uses experience to determine the best way to collect data quickly and "accurately" according to his or her definition. There is a great need not only to standardize data collection processes, but also to eliminate human error induced by lack of experience or fatigue. This research proposes a fiber optic based monitoring system as a possible solution to eliminate a number of problems with current cellular data collection methods and to increase the data collection rate tremendously since the process could be automated.

Acknowledgments

I would like to thank:

Dr. Richard Claus, my chair, for his invaluable direction and exemplification of an engineer.

Dr. Kent Murphy for showing me that we can become anything we strive for.

Dr. Thomas Toth for his continual encouragement and discussions on interfacing optical fibers with in vitro cell culture observation.

Carvel Holton for technical discussions.

Dr. Carlos Suchicital for providing support.

Laura Douglas for keeping me supplied with cells to study and for technical discussions.

Shawn Walker for asking me questions.

Dr. John Kenney for supplying me with the skill necessary to attempt this undertaking.

My family for understanding what this required.

I would not have been able to complete this project without the integral support of those around me. Your support, and encouragement was instrumental in the culmination of this research. I am truly thankful.

Dedicated to my loving wife: Lisa West

TABLE OF CONTENTS

LIST OF FIGURES

LIST OF TABLES

Definitions:

Owing to the fact that two seemingly unrelated fields are being brought together to achieve a new measuring instrument, a definitions section is included to help both sides read the text understandably.

achromatic - without color *A lens without color is able to resolve just the cells impact on light interaction.*

Airy disk - When light passes through circular aperture a diffraction pattern is established of light and dark, concentric, intensity rings, the bright maxima at the center is the Airy disk.

bandpass filter - a device that allows only a certain frequency, or number of frequencies, to pass

chromatic - having color *These lenses would induce color into the readings because they were colored.*

concave - curved inward *A concave lens is curved inward on both sides.*

convex - curved outward *A convex lens is curved outward on both sides.*

dark current - output of a photodetector without illumination

evanescent field - the light energy that is propagating in the cladding of optical fiber

in vitro - in glass or a vessel

in vivo - in a living organism

morphological - relating to the form and structure of an organism

n - refractive index

numerical aperture - the sin of the maximum input angle that a cone of light will enter multiplied by the refractive index of the lens being entered (NA = $n_0 \sin\theta_{max}$)

photodetector - a device that produces an output current proportional to the light level impinging on the surface of the detector

planoconvex - having one plane, flat, surface and one curved inward surface

quantum efficiency - in detectors it is the ration of current produced to incident light flux

spherical aberration - a defect that will not allow the lens to focus a clear image on a plane, on-axis surface from a point source object

subscripts - i incoming or interface, t transmitted, r reflected, perpendicular, $\parallel$ parallel

translucent - shining through

1. INTRODUCTION

Historically, observations of cells and cell cultures have been performed using the light microscope, an instrument which was invented somewhere around 1590 by Hans and Zaccharias Janssen while other opticians developed it around 1610. Johannes Kepler devised a compound lens system using a convex lens in the eyepiece around 1611. The microscope slowly evolved and practitioners of the device were termed “microscopists”. Robert Hooke popularized the instrument when he published *Micrographia* in 1665. Early forms of the microscope were nothing more than a convex lens inside a movable tube that could slide the convex lens closer and farther away from the viewed object (Figure 2).

Different ideas were employed to improve the resolution. Hooke attached a focusing collar to the lens in 1664. Johannes Hevelius improved this by adding a fine adjustment to the focusing collar, using a lead screw, in 1673. In 1693 John Marshal placed the specimen on a stage and moved the stage with respect to the lens to improve resolution. Bonanni was a significant contributor to the development of earlier microscopes and one of his novel microscopes is shown in Figure 3. Lenses were chromatic until 1824 when William Tulley developed the achromatic lens. Spherical aberrations were the main contributor to slowing the resolution progress in microscopy. The achromatic lens was capitalized on by Joseph Jackson in 1827. He combined two planoconvex achromatic lenses to almost eliminate the spherical aberrations from lenses produced at that time.

Since cells are often colorless and translucent, a number of microscopic methods have evolved to resolve the image being viewed. The practical resolution limit of a light microscope is 0.2 μm. This is calculated at the smallest wavelength of visible light (violet 0.4 μm) and an oil immersion lens having a numerical aperture of 1.4.

$$\text{resolution} = \frac{0.61\lambda}{n \sin\theta} \tag{1}$$

where λ is the wavelength of incoming light, n is the refractive index of the lens, θ is the maximum input acceptance angle. Refractive index is defined by

$$n = \frac{c}{v} \tag{2}$$

where c is the speed of light and v is the velocity of light in the medium. The maximum numerical aperture (NA) a dry lens can attain is one.

$$NA = n \sin\theta \tag{3}$$

where n is the refractive index of the lens, and θ is the maximum input acceptance angle.

Significant improvements have been made to the viewing process, such as the Abbé microscope by Zeiss in 1886. In 1930 Lebedeff designed the first interference microscope and in 1932 Zernicke designed the phase-contrast microscope. Nomarski devised the differential contrast system in 1952, and in 1981 Inoué and Allen invented video-enhanced contrast microscopy. The confocal scanning microscope became commercially available in 1988. Fluorescence microscopy, phase-contrast microscopy, differential-interference-contrast microscopy, and dark-field microscopy all take advantage of the interference and phase effects of light interacting with the sample to bring out specific cellular details thus improving resolution. Differential-interference-contrast microscopy combined with electronic imaging techniques improves the resolution to 0.025 μm. Scanning electron microscopy improved the resolution three orders of magnitude greater: 0.1 nm.

Figure 4 shows the similarities in the lens arrangements of a light microscope and an electron microscope. Figure 4(A) is the light microscope and figure 4(B) is the electron microscope. Confocal scanning microscopes (Figure 5) have the ability to view three-dimensional images using the same premise as a fluorescence microscope. A laser light source scans through the sample and unwanted light rays are deflected by using confocal pinhole plates in front of the laser and detector. Computer-based image processing enables this technique as light is scanned through the sample from bottom to top.

While microscopes have undergone tremendous resolution improvements and allow scientists to observe minute details of biological activity, there are discontinuities in the data collection process that arise from a variety of sources. Multiple samples are grown in separate culture vessels and biological activity in the vessel is observed and it is assumed that activity progresses in a similar fashion in all the vessels. The overall process can be viewed using a phase-contrast or a differential-interference-contrast microscope, and microcinematography may be used to collect data points. Unfortunately, archiving of the video images results in a large amount of data storage, and human intervention is required to interpret all the hours of captured images.

If microcinematography is not available, the researcher is exposed to long, tiring hours of manual data collection. Lack of experience, individual analysis style, incorrect data entries, and incorrect data calculation also contribute to large variations in data values. To obtain consistent results, the biological system would ideally be left in its natural habitat with very little human interaction involved in the data collection process. This option is not often available because biological systems under study are not directly accessible to monitoring equipment. Researchers must settle for indirect readings by collecting samples of cells grown outside of their natural habitat, or harvesting accessible cultures for observation. Current monitoring processes do not provide objective, in-situ observations of the many cellular processes.

Cost is another factor, leading to discrepancies in the analysis of cellular activity. Tests are multistep, requiring expensive equipment, chemicals, and many work hours for only a few data points. Certain steps in the data collection process may be automated, but not everyone can afford this; therefore, many of these tests are performed manually thus subjecting them to human error.

1.1. BIOSENSORS

New observation techniques need to be developed that allow biological systems to be monitored without direct human interaction. This would eliminate many of the downfalls from current methods. Novel work has already been accomplished in this area using a polymer matrix attached to fiber endfaces to monitor the contaminants in a hazardous environment achieving a resolution in the parts per million level.[1] Devices of this type are termed "receptor site" biosensors and are used for monitoring specific biological components via molecular kinetics. Biomolecules attached to the fiber are active sites for the sensor. Types of biomolecules currently included are chelators, enzymes, receptors, antibodies, and ionophores.[2] The receptor's structure determines the sub-group of the biosensor (i.e. a biosensor using an antibody receptor is termed an immunosensor.) This biological detection mechanism is used to induce signals to a transducer which in turn produces a usable output. The two general classifications of biosensors are electrical and optical. Electrical transduction type sensors measure changes in voltage (potentiometric), current (amperometric), or resistance (conductometric), and piezoelectric sensors measure the change in oscillation frequency of a piezoelectic crystal. The biosensing market is predicted to reach a value of $895 million by the year 2000[3], but it is 1998 and only one item is enjoying commercial market success, the "glucose pen" by Exactech.[4]

The intended community of biosensor users has agreed on certain characteristics that biosensors should possess: 1) the binding method should be mechanistically reliable, 2) have a rapid response time, 3) have a high specificity for the intended biomolecule, 4) have a rapid response time, 5) be reusable and cost effective, 6) be small, 7) produce reproducible data, 8) have in vivo sensing capability, 9) and be able to detect multiple analytes.[5] Fiber optical sensors are able to meet all the requirements of the consensus for biosensors.

Conductometric biosensors consist of electrodes immersed in solution. One electrode is coated with a binding agent. As the intended biomolecule attaches to the electrode the change in resistance through the solution is measured. This type of biosensor is used in ionic solutions.

Amperometric biosensors measure the current between two electrodes. Catalysts are placed in the well to balance the electron flow and improve response time. The biomolecules studied in this technique are ion channels, enzymes, and receptors.

Potentiometric biosensors measure the potential at an electrode. The electrode potential is compared to that of a reference electrode. Fluctuations in charge density at the sensing electrode are used to determine Redox potentials, transmembrane potentials, and pH.

Piezoelectric biosensors are possible because the crystal's oscillation frequency is mass dependent. The crystal is coated with a receptor coating. As the biomolecules bind the coating, the mass changes in the crystal; therefore, the oscillation frequency changes. This change in oscillation frequency is measured and correlated to the amount of material bound to the receptor sheet.

Electrical biosensors work, but their results are hard to characterize. Fluctuations in readings cause irreproducible results. They are used mainly in simple systems where hundreds of tests have been performed to determine their "characteristic" response to the intended system. They are solution based mechanisms and not suited for in-vitro applications. To answer this need, fiber optical sensing systems are best suited.

1.2. FIBER OPTIC SENSORS

Fiber optical systems are an non-invasive means of determining biological activity. They are immune to the problems plaguing electrical biosensors, such as interference from voltage surges, radio frequencies, electromagnetic radiation, and corrosion. Their size makes them perfect for in-vitro or in-vivo studies of biological activity. They also possess the capability of being sterilized, an important consideration in cell culture analysis. There are two regions of measuring signal interaction: 1) at the distal tip of the fiber, also called optrode configuration, and 2) the evanescent field along the fiber (Figure 6).

The fiber is coated with a receptor biomolecule at either place. The sensor can either be active or passive. In the passive configuration, fluorescing biomolecules transfer their information to the fiber via the evanescent field, or the distal tip. In the active configuration, light is sent down the fiber using a light source and changes in reflected light are measured. Three geometries exist for fiber optic biosensors using the evanescent field mechanism. The step etch provides a stronger signal than just exposing the sensing region to the evanescent field. Tapering the fiber improves the signal, and the current optimization of the signal is achieved by combining the two into a combination taper (Figure 7).

The evanescent field of an optical fiber has an exponential decay of energy extending from the core - cladding boundary and into the surrounding medium. The depth of the field into a surrounding solution, using a quartz fiber, is about the same as molecular dimensions for immunological systems.[6]

$$E = E_0 \exp\left(\frac{-z}{d_p}\right) \tag{4}$$

where E is the energy of the evanescent field, E_0 is the energy originally put into the fiber, z is the distance of the cell from the outside surface of the fiber, and d_p is the penetration depth of the field into the medium. The penetration depth of the field into the medium is given by

$$d_p = \frac{\lambda}{\sqrt{2\pi\left(n_1^2 \sin^2\theta_1 - n_2^2\right)}} \tag{5}$$

where d_p is the penetration depth of the field into the medium, λ is the wavelength of light being used, n_1 is the refractive index of the core, n_2 is the refractive index of the cladding, and θ is the angle the light is making with respect to the interface of n_1 and n_2. Realize that input energy and wavelength can be changed to increase the evanescent field's depth into the medium.

Light is an electromagnetic wave and an optical fiber imposes boundary conditions on the number of waves that are allowed to travel down it. These combinations of waves are called modes and the number of modes able to propagate down a step - index multimode optical fiber is given approximately by the V number, given by

$$V = \frac{2\pi r}{\lambda}\sqrt{n_1^2 - n_2^2} \tag{6}$$

where r is the fiber radius, λ is the wavelength of light being used, n_1 is the refractive index of the core, and n_2 is the refractive index of the cladding. To match the propagation conditions between the fiber and a surrounding solution requires a reduction of the fiber radius, allowing the modes traveling in the cladding (evanescent field) to be coupled constructively with the solution.

$$r_{matching} = r_{cladding}\sqrt{\frac{n_1^2 - n_2^2}{n_1^2 - n_3^2}} \tag{7}$$

where n_1, n_2, n_3 is the refractive index of the core, cladding, and solution respectively. This is matching the modes of the waveguide to the modes that will penetrate into the solution, thereby increasing resolution because the waves are not destructively interfering at the interfaces.

The reason the combination taper works best is because the step index method results in the loss of most of the input light intensity at the junction, and the taper mode does not achieve effective matching until half of its length. The combination taper is a very effective compromise. The internal reflection method has been applied to total internal reflection fluorescence (TIRF) of biomolecules and the evanescent field method is applied to attenuated total reflection (ATR) systems; both methods have shown success.[7,8] Unfortunately, current fiber optic based biosensors do not help scientists trying to observe events at the level of whole cells.

To answer this need, novel fiber optic based systems are proposed as a method for data collection. This work originated from a project named “Aspires”, which is an interdisciplinary program, at Virginia Tech, designed to incorporate expertise from different fields to solve current technological problems. Projects goals were to design a fiber-optic system capable of monitoring biological phenomena. The system had to 1) be an inexpensive set-up, 2) continuously monitor a biological environment, 3) not disturb the cells while monitoring, and 4) have the capability for automation.

To better understand how fiber optics could be used to monitor cell cultures, one must first understand the basics of optical theory affecting the proposed design. The Fresnel equations for transmittance and reflectance are the basic building block for these devices. These equations allow the flux densities to be separated. The Fresnel equations for reflectance and transmittance (equations 16, 17) can be derived starting from the Fresnel formulas for perpendicular and parallel incident and reflected waves, as follows. Assume that the incident wave electric field is monochromatic and perpendicular to an isotropic media. The magnetic field component is parallel to the boundary. Also assume the normal component of the magnetic field and the tangential component of the electric field is continuous across the boundary.

$$\hat{\mathbf{k}} \times \mathbf{E} = \upsilon \mathbf{B} \tag{8}$$

where $\mathbf{k}$ is the unit propagation vector, $\mathbf{E}$ is the electric field vector, υ is the speed of the field in the medium, and $\mathbf{B}$ is the magnetic field vector. At the boundary, the condition exists of

$$\mathbf{E}_{0i} + \mathbf{E}_{0r} = \mathbf{E}_{0t} \tag{9}$$

where $\mathbf{E}$ is the electric field, i is incident, r is reflected, and t is transmitted. A monochromatic lightwave is of the form

$$\mathbf{E}_i = \mathbf{E}_{0i}\cos\left(\mathbf{k}_i \;\; \mathbf{r} - \omega_i t\right) \tag{10}$$

$$\mathbf{E}_r = \mathbf{E}_{0r}\cos\left(\mathbf{k}_r \;\; \mathbf{r} - \omega_r t + \varepsilon_r\right) \tag{11}$$

$$\mathbf{E}_t = \mathbf{E}_{0t}\cos\left(\mathbf{k}_t \;\; \mathbf{r} - \omega_t t + \varepsilon_t\right) \tag{12}$$

where $\mathbf{E}$ is the electric field, i is incident, r is reflected, t is transmitted, $\mathbf{k}$ is the wave vector, $\mathbf{r}$ is the position vector, ω is the angular frequency, t is time, and ε is the phase constant. At the interface, the cosine terms are equal and conservation of energy holds true (equation 9); therefore,

$$\left(\frac{\mathbf{E}_{0r}}{\mathbf{E}_{0i}}\right) = \frac{\dfrac{n_i}{\mu_i}\cos\theta_i - \dfrac{n_t}{\mu_t}\cos\theta_t}{\dfrac{n_i}{\mu_i}\cos\theta_i + \dfrac{n_t}{\mu_t}\cos\theta_t} \tag{13}$$

where n is the refractive index and μ is the permeability.

$$\left(\frac{\mathbf{E}_{0t}}{\mathbf{E}_{0i}}\right)_{\perp} = \frac{2\dfrac{n_i}{\mu_i}\cos\theta_i}{\dfrac{n_i}{\mu_i}\cos\theta_i + \dfrac{n_t}{\mu_t}\cos\theta_t} \tag{14}$$

where the component designations are the same as in previous equations. Figure 1 would be helpful in visualizing the field incident upon the interface. The perpendicular and parallel components are not separated, but the diagram is sufficient for a general understanding. These component designations will hold for equations used throughout the text.

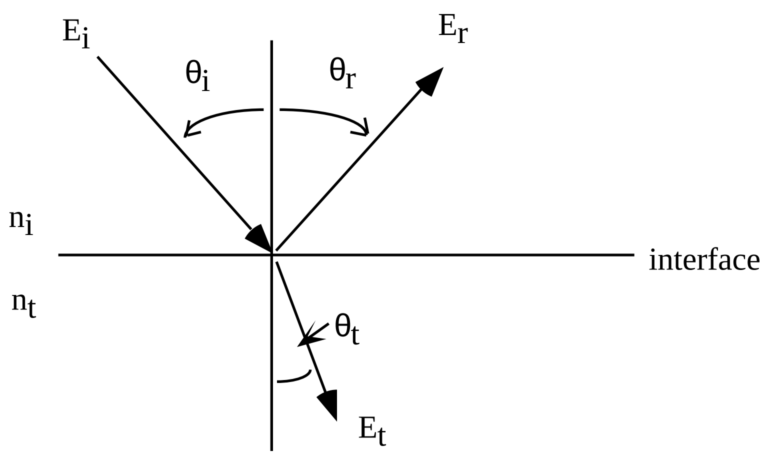

Figure 1. Diagram of electromagnetic field incident upon an interface of two homogeneous, lossless, dielectric media.

Since both experimental configurations use the perpendicular component of the light, only the perpendicular equations will be explored. The amplitude of the reflection and transmission components are of concern. Two situations are in effect. In situation 1, a 1300 nm laser is generating the beam to be reflected; it is monochromatic. In situation 2, a light emitting diode is shining down upon the sample plate. In situation 1 reflectance is measured with a photodiode, and in the second situation, transmittance is calculated with a computer program after being detected by camera.

The irradiance (I) over a cross sectional area is given by

$$I = \frac{c\varepsilon_0}{2} E_0^2 \tag{15}$$

where c is the speed of light and ε is the permeability of the medium. The total reflectance (R) and transmittance (T) are the ratios of reflected, or transmitted flux to incident flux.

$$R \equiv \frac{I_r \cos\theta_r}{I_i \cos\theta_i}\text{, and} \tag{16}$$

$$T \equiv \frac{I_t \cos\theta_t}{I_i \cos\theta_i}\,. \tag{17}$$

The energy flowing into the system must equal the energy flowing out

$$I_i A \cos\theta_i = I_r A \cos\theta_r + I_t A \cos\theta_t \tag{18}$$

where A is the cross sectional area.

After considerable manipulation with the assumptions that the environment is homogeneous, isotropic, dielectric, and $\theta_i = 0$, the desired equations are obtained

$$R = R_{\parallel} = R_{\perp} = \left(\frac{n_t - n_i}{n_t + n_i}\right)^2 \text{, and} \tag{19}$$

$$T = T_{\parallel} = T_{\perp} = \frac{4 n_t n_i}{\left(n_t - n_i\right)^2} \text{.} \tag{20}$$

The refractive index is measured as a function of reflected light intensity in situation one. Situation two measures the light transmittance through the sample as a function of refractive index.

When using a 96 well plate, some effects need to be considered; occasionally, a bubble will form in the solution and connect to the inside of the lid. Condensation will also form on the inside cover of the 96 well plate after it has been out of the incubator for a couple of minutes. The bubble will cause an interference fringe based upon the equations

Bright fringes: $$2d = \left(m + \frac{1}{2}\right)\lambda_n \qquad m = 0,1,2,\ldots, \tag{21}$$

Dark fringes: $$2d = m\lambda \qquad m = 0,1,2,\ldots \tag{22}$$

where d is the film thickness, λ is the wavelength of light, and λ_n is the wavelength of light in the media according to

$$\lambda_n = \frac{\lambda}{n} \tag{23}$$

where n is the refractive index of the thin film. The 1/2 is introduced in equation 21 because the wave reflecting off the back surface of the thin film undergoes a phase change of 180°. Figure 8 shows bright and dark fringes produced by optical phase differences.

An optical fiber-based system could be designed to monitor the life and death cycles of cells in vitro or in vivo. One method might have the fiber sensor inserted into the cell culture vessel to end just above the monolayer and observe the life and death cycle of cells directly in vivo, without human intervention. Another method would place the end of the fibers below the cell culture vessel and observe the cellular processes through the wall of the cell culture vessel. Because optical fibers do not suffer the same effects of signal degradation electrical observation methods do, such as charging by induction, crosstalk, voltage surges, and temperature effects, the results would be more precise. Cellular processes could be monitored from the start to the finish, using fiber optic sensors, with a computer as a data collection device. The second novel method of data collection would use high numerical aperture optical fibers. Data collection using this method would be a simple process, involving little effort on the experimenter’s part. The 96 well plate, or flask, would be placed on the viewing fixture and a computer would collect data from a camera using a frame grabber. This data collection process eliminates a great deal of experimental error contributions resulting from the human element and allows the in vitro, macroscopic measurement of cellular processes. The sensing area is determined by the size of the fiber bundle used to make the observations and resolution can be increased by choosing appropriate fiber bundles.

1.3. CELLULAR REPLICATION

Cellular replication can be divided into two division processes, namely mitosis (nuclear division) and cytokinesis (cytoplasmic division). In eukaryotic mammalian cells, division is usually symmetric. The process can be classified in six steps; prophase, prometaphase, metaphase, anaphase, telophase, and cytokinesis. During prophase, prometaphase, and metaphase changes to the cell are internal. In the anaphase, telophase, and cytokinesis, the cell is dividing and actually changing shape with consequential changes in refractive indices. These stages should produce changes in light interacting with the cells, at least between the stages of mitosis and cytokinesis (Figure 9).

1.4. FIBROBLAST AND EPITHELIAL CELLS

Fibroblastic cells are from the connective tissue family of cells. They are fibrous in nature and their ability to withstand injuries, along with an abundant replication rate, makes them one of the most used cells for culture studies. They are a plate-like cell with “arms” for connecting different tissues. Fibroblastic cells require an anchorage point to divide, and cells that are suspended in solution only have an 8% chance of entering the S phase.[9] (The S phase is the stage of mitosis where the cell replicates its chromosomes.) Fibroblastic cells will continue the replication process until a confluent monolayer, i.e. the cells are touching each other, is formed on the surface of the object adhered to, or until senescence is reached.

Fibroblastic cells live in a variety of environments but epithelial cells are a more specialized, polarized cell type. They serve as linings, growing in sheets, and deliver specific products out both surfaces of the cell. An example of epithelial cells is the lining of mucus membranes, or the lining of the gut. Epithelial cells lining the gut secrete digestive enzymes from their basolateral surface to repair the stomach lining (Figure 10). The cells used in this study were fibroblastic green monkey kidney cells (VERO), epithelial rhesus monkey kidney cells (LLC-MK_2 and CV-1), and human thymidine kinase negative human cells ($HuTK^-$).

2. MATERIALS AND METHODS

2.1. Treatment of Cells

Four types of eukaryotic mammalian cells were used in the research (CV-1, VERO, LLC-MK_2, and $HuTK^-$). Standard aseptic procedures were used for passing and maintaining the cell cultures. Cells were grown in 1x Eagles Minimal Essential Media (EMEM) containing 5-10% Fetal Calf Serum (FCS), 1 x L-Glutamine. In some cases, a 2 x concentration of antibiotics of streptomycin, amphotericin, and penicillin were added to the median to protect the cells from infection.

A sterile 10 mL pipette was taken from the sterile storage container and flamed to prevent contamination. One of the 75 mL flasks containing the desired cells was opened and the media was suctioned off with the pipette and discarded into a bleach solution. The 10 mL pipette was placed into the bleach solution outside of the hood and a 1 mL pipette was taken from the sterile storage tube. After being flamed, it was allowed to cool. Then 1 mL of Trypsin was added to the cell flask. The Trypsin was washed along the back of the cell flask and then the flask was allowed to set for about one minute to let the Trypsin digest the cellular matrix holding the cells to the back of the flask. The 1 mL pipette was placed into the bleach solution outside of the hood. After a short wait, the flask was rapped and observed to determine if the cells were free from the back of the flask.

A 5 mL pipette was taken from the sterile storage tube and flamed. It was allowed to cool, then 5 mL of media (Fetal Calf Serum, and 1x Eagles Minimal Essential Media (EMEM), 10% Fetal Calf Serum (FCS), 1 x L-Glutamine) was washed down the back of the flask. The media was suctioned up again and this procedure was repeated two times. After the third suction, the pipette was butted against the bottom of the flask and the media was forced against the bottom of the flask, this was to break up any cellular clumps that might exist. The cells were suctioned up again and sprayed forcefully onto the bottom of the flask again to mix them. The cells were then deposited into a 25 cm^2 flask, or a 96 well plate, depending on the experiment.

For experiments using the 25 cm^2 flask, cells were placed into the flask at a high seed density and media and antibiotics were added to bring the liquid level of the flask to a level where it was almost touching the lid of the flask when the flask was laying on its bottom. For experiments using the 96 well plate, three different cellular densities were deposited into the well plate. Wells A1 and C1 had cellular densities of 100,000 cells/well, wells A3 and C3 had cellular densities of 10,000 cells/well, and wells A5 and C5 had cellular densities of 1,000 cells/well. The wells were filled with media to a volume of 300 μL/well.

2.2. Monitoring the Impact of Cellular Processes on Refractive Index using a Fiber Optic Sensing System

A laser diode, 2x2 biconical coupler, photodiode, an oscilloscope, a function signal generator, and a lock-in amplifier were configured according to Figure 11. These items work together to resolve a voltage from an optical signal injected into an optical fiber. Several 1300 nm, single mode, polyimide coated, optical fibers were cleaved to have a highly reflective character. After cleaving, the individual fibers were calibrated to establish their individual response to changes in refractive indices. The only reason of having several fibers was in the event of one breaking, there would be extras. A fiber was connected to the fiber optic sensing system and a baseline reading of the fiber in air was taken. Then the endface of the fiber was immersed in the first refractive index oil of 1.330 ± 0.002. After a reading was taken, the endface of the fiber was cleaned with a Kimwipe wetted with alcohol. The fiber was determined clean if the reading in the lock-in amplifier returned to the original starting position. This method ensured all the previous refractive index oil was off the fiber, the next reading was an accurate reading of the oil, and cross contamination of oils did not occur. The fiber was then inserted into the next higher refractive index oil and a reading was taken, then the fiber was cleaned. This process continued, in refractive index oil steps of 0.02, for a range of 1.330 - 1.632.

After calibration, the fiber sensor was autoclaved to ensure sterility before insertion into a cellular environment. The fiber was inserted into the ventport of a 25 cm^2 flask containing cells, media, and antibiotics. The fiber was held in place with a dab of nail polish placed where the fiber was inserted into the ventport of the flask. The nail polish had a two fold purpose; one, it held the fiber sensor in place and two, it sealed the hole made in the vent port of the flask cap after fiber insertion. The sealing of the hole helped maintain cell culture sterility. The flask was kept on the heated stage (37.1° C) of the light microscope during experimental runs. The output voltage of the photodiode was monitored using a lock-in amplifier and readings of the photodiode output were collected in 2, 4, and 8 hour increments. It was established that the four hour increment worked best.

2.3. Monitoring the Impact of Cellular Densities on Transmittance using a Fresnel Fiberscope

The 96 well plate containing cells was kept in an incubator (37.1° C) until data analysis points were collected. For collecting data, the 96 well plate was taken out of the incubator and the masking plate was placed underneath. The plate was placed on the Fresnel Fiberscope's viewing stage and aligned for maximum transmission of light through the well plate. After alignment, a picture of the output ends of the optical fibers was taken using a computer, frame grabber, and CCD camera. The frame grabber was set to capture 620 x 480 images, saved in TIF format, because the software was optimized for that image size.

The plate, and the masking plate, were then moved, as a unit, to the light microscope and corresponding image points were collected with the same image capturing equipment by moving an AB switch to the appropriate setting (Figure 12 Block diagram of the Fresnel Fiberscope set-up.). The data was transported to a Power PC, using ZIP disks, and evaluated using NIH Image software. Images were imported into the NIH Image software program and density calibrated using an internal Rodbard equation standard. The equation was optimized for measuring pixel area resolutions evaluated using NIH Image. The images were then measured with the internal scale set to pixels.

3. INSTRUMENT DESIGN

3.1. Fiber Optic Sensing System for Measuring Refractive Index Changes

A light source, 2x2 coupler, detector, and necessary support equipment were configured for the measurement of refractive index changes from the experimental flask. A 1300 nm single mode, step index, polyimide coated optical fiber was inserted into the flask through one of the "breathing" ports on the flask lid. A 1300 nm laser was fed into the sensing fiber via a 2x2 bi-directional coupler. (One end of the coupler is the sensor and the other fiber of the coupler is shattered to ensure no back reflections.) Refractive index changes on the sensor's end were monitored with a photodiode. The photodiode produces a voltage output proportional to input signal intensity. This voltage is processed by a lock-in amplifier, which also displays the measured voltage changes. A similar experimental arrangement was used to measure the cure rates of epoxy.[10] Using the fiber optic sensing system method, index of refraction changes are measured over cellular lifetimes.

During monitoring, the reference and output signals were fed into an oscilloscope for simultaneously monitoring of the signals. This had the benefit of viewing if the fibers were coupled properly at the bulkhead. If the fibers were not fully inserted into the bulkhead, or if dirt was on the endface of the fiber, the oscilloscope displayed a sinusoidal waveform with significant decrease in amplitude compared to the reference signal. This enabled a "standard" connection to be established. The experimental set-up for measuring the refractive index changes is displayed in Figure 13.

The photodetector has an inherent spectral sensitivity; therefore, the photodetector is chosen to have its largest gain at the wavelength of the incoming light. Figure 14 shows the spectral sensitivities for different photodetectors. As can be seen, the best photodetector for this application is either a Ge or InGaAs photodetector. The quantum efficiency is higher for the InGaAs photodetector (0.6 responsivity verses 0.5 for a Ge photodetector), but the cost is also inherently higher. Since the signal to noise ratio is small, an InGaAs photodetector is used. The InGaAs photodetector had a 75 μm active area, this small area reduces the dark current contribution to the signal noise.

3.2. SIGNAL TO NOISE RATIO

The signal to noise ratio is low in this case because the incoming signal is very weak compared to the background noise signal. Since the signal to noise ratio is small, a function signal generator was used to modulate the laser diode current at 400 Hz with a DC offset of 2.5 VDC. A lock-in amplifier tracked the modulation signal and separated the actual signal from the modulation signal. The lock-in amplifier was used as a bandpass filter to allow the actual output signal to be resolved from the noise level.

3.3. SENSOR HEAD

The actual sensor head is a cleaved fiber end. The fiber used was polyimide coated to improve the chance of functioning in the different cellular environments. After the end was cleaved it was checked using an interferometer to ensure a “good” cleave. This is determined from the interference pattern generated by the interferometer. The fiber used for sensing in these experiments generated two interference fringes. With this particular interferometer, three interference lines are the maximum to ensure a good cleave. After checking with an interferometer, the fiber was immersed in Cargille calibrated refractive index oils between the values of 1.330 (±0.0002) - 1.632 (±0.0002) to determine the fiber’s individual response to different indices of refraction. Calibration is important because even if the fiber is cleaved the same way, it does not really have the same endface angle every time. The reflections are angle dependent and this requires each cleave to be calibrated. Figure 15 is a general refractive index verses output voltage graph for a fiber sensor head.

4. FRESNEL FIBERSCOPE DESIGN

4.1. MOTIVATION

The author knows of no current methods of macroscopic monitoring of morphological changes relating to cellular activity. These types of readings could be very revealing as to the actual cellular events. Cellular processes are known from prior work with individual readings taken at specific points in time of cellular systems, but the author does not know of any procedures to macroscopically monitor the entire process in vitro. Using conventional observation techniques the stages of prophase, prometaphase, anaphase, etc. are fairly well understood, but the inability to macroscopically monitor cellular lifetimes leaves large unknowns in the study of viral effects on cellular processes.

Another unknown in the study of cellular activity is the effect of gravity on cellular processes. Data acquisition of eukaryotic cellular processes is difficult in space. Current cellular observation methods require interaction with the cellular environment. This is not conducive to study on space flights; not only may the crew be exposed to biological risks, but the usual methods of administering various media onto viewing plates would pose considerable difficulty in a weightless environment. There is also the issue of experience. To conduct exacting cellular studies requires a great deal of experience on the researcher's part when "judgment" is called for. It is very unlikely someone with a high level of experience in the biological, or virological, field would be able to qualify for space missions. On the other hand, data accumulated automatically in space and made available either “live” during the flight, by transmitting the data while it was occurring, or after the flight concluded would allow such experiments to be performed in space.

The idea of Fresnel Fiberscope came to the author while trying to solve the problem of macroscopic, in vivo, cellular monitoring. It is called a Fresnel Fiberscope because it uses an optical fiber array to monitor cellular morphology based upon the Fresnel equation for transmittance as a function of refractive index (see below), thus it seemed appropriate to call the device a Fresnel Fiberscope.

$$T = T_{\parallel} = T = \frac{4 n_t n_i}{\left(n_t - n_i\right)^2} \qquad (24)$$

Measuring the refractive index changes of cells over time seems to be a good idea. Reflectance and transmittance are a function of refractive indices as seen in equations 19 and 20. Using a fiber optic sensing system with the fibers embedded into the vessel for in vivo monitoring of cell morphology suffers from a small viewing area. It is also important to keep the fiber immobilized during experimental runs. Cells “move” as they replicate. If they migrate, the readings could be of different cells at each reading. If it is used for in vitro sensing each flask, or 96 well plate, would have to be embedded with optical fibers. Current flasks and 96 well plates are disposable, and this would push the construction costs up tremendously if they had to be imbedded with optical fibers. To try to improve on these shortcomings, a slightly different approach is considered.

4.2. THEORY

Cells are cultured in a 96 well plate. This will be the environment that will be monitored using the proposed device. A light source shines down on the 96 well plate at a distance sufficient enough to assume the incident light waves are planar. As the light passes through the sample, the transmittance is changed. High numerical aperture optical fibers are mounted underneath the plate and are used for collecting the light passing through the cellular environment. Any changes the environment has on the light passing through the environment is seen by differences in intensity on the output end of the fibers. This difference in intensity changes are currently monitored using a Charge-Coupled Device (CCD) camera. A CCD camera was chosen because it allows an inexpensive method to determine if the idea would actually work. A more accurate method would be to attach the output end of each individual fiber to a photodiode, then the voltage changes of the photodiode could be monitored. This would increase resolution, but it would also require much greater funding.

The heart of the Fresnel Fiberscope is the fiber optic bundles and the viewing camera. A CCD camera with an iris lens was used to monitor the intensity changes on the endfaces of the optical fibers. This data was fed into a computer for storage, but presently data is still manually collected. Intensity changes are correlated to cellular changes and recorded optically via a CCD camera mounted on a microscope. After an intensity reading was taken, the 96 well plate was moved to a light microscope and correlating points on the 96 well plate were digitally photographed. The data was fed into the same computer and an AB switch allowed the computer to monitor the light microscope's camera or the Fresnel Fiberscope's camera. (Figure 17 Drawing of the Fresnel Fiberscope box. Figure 18 Internal picture of the Fresnel Fiberscope.)

5. EXPERIMENTAL RESULTS AND CONCLUSIONS

5.1. DESIGN INVENTION

The type of optical fibers to be used had to be decided. Since the goal of this project was to have a more macroscopic representation of cellular environments, a high numerical aperture fiber was decided upon. A polymethyl-acrylate optical fiber sheathed with a flourine doped polymer was used to capture the incoming light (Edmund Scientific - part number P53,832). It was chosen because it possesses an acceptance angle of 35°. This would allow fewer fibers to be used in observing a larger area of the cells.

The next question to be resolved was how the fibers would be held in a constant position in relationship to the positions on the underside of the well plate. The first idea was to just cleave them and leave the jacket as a separating layer between the fibers, however, if the endface of the fibers were cleaved at different angles, the input intensities to the CCD camera would be different. This effect arises because the numerical aperture is angle dependent. If the heads of the optical fibers were cleaved at different angles, their numerical aperture would be different; therefore, their response to incoming light would be different. Epoxy was used in the next attempt of holding the optical fibers in a specific location. The fibers were stripped of 1/2" of the jacket and inserted from the bottom of the 96 well plate and into the epoxy. The epoxy chosen was a Devcon "Plastic Welder". It appeared opaque to the naked eye, but when a light source was shone on the endfaces the contrast disappeared. The epoxy was translucent! An opaque epoxy was used next (Miller-Stephenson Epoxy 907), thus restoring the contrast. Then the question arose as to how would the fiber positions be exactly correlated to the bottom of the well plate.

A correlation chart (Figure 19) was made by comparing the manipulation of the input light intensity of each single fiber and monitoring the output image. This allowed the accurate determination of the input endfaces of the optical fibers to be matched to the output image, but how was the image of the well plate on the microscope going to be correlated to the image obtained from the fiber bundle? It would be very easy to have the well plate off angle by a few degrees. This would have detrimental impacts on the correlation of measured images to the actual cellular picture captured by the light microscope.

To correct this problem, a masking plate was machined to correlate the exact fiber placement to its physical location on the well plate. The plate was fabricated at a local machine shop. To correctly drill the holes, a template needed to be made of the fiber positions. A dowel of dark gray poly-vinyl chloride (PVC) was inserted into a 96 well plate, and holes were drilled through the material at the exact positions the optical fibers would be inserted into. The masking plate was secured underneath and it was drilled through after the drill bit passed through the PVC. This would allow the machinist to know where the fibers would be placed, and accurately align the masking plate holes. This method had an unforeseen advantage of not only making a mask, but the fibers had a holding template to be placed into. The epoxy filled wells were then replaced with wells holding PVC blocks. Now the fiber placement in all the wells were the same, and the diameter of the holes in the mask exactly matched the diameter of the fibers. After using the improved well plate, and mask, another effect was seen; diffraction from the internal edges of the circular aperture shadowed the fiber and induced error. To resolve this, the diameter of the holes in the masking plate were increased from 0.040” ±0.001 to 0.048” ±0.001 in. The exact diameter of the holes, after drilling, were checked with an Ex-Cell-O contour projector. The results of increasing the diameter of the holes in the masking plate was to place the Airy disk over the endface of the fibers.

Determining the most appropriate light source was a big problem. Using a halogen 50 watt bulb controlled by a dimmer switch was the original idea. A voltmeter, with an accuracy of ±0.001 VDC, was used to determine the input voltage to the halogen bulb to ensure the same output intensity while taking measurements. It was later realized that the voltmeter was not measuring the output intensity of the halogen light source. Its only function was to measure the input voltage to the light source. The effect of resistive heating was realized at this point because at low input voltages the output intensity of the halogen bulb was seen to fluctuate. Fluctuations in the light source intensity would nullify the validity of data among consecutive readings. The filaments of the light source are resistive in nature and their resistance to power makes them luminesce. The graph of input power verses output intensity is based upon an exponential relationship at the lower end of the graph and a more linear relationship at the upper end. Unfortunately the light level needed was on the part of the curve that was the most sensitive. To circumvent this problem, the ambient room light was tried as the light source. This did give controllable light intensity because when all the room lights are on, the intensity will always be approximately the same. One of my advisors asked about someone repeating the experiment elsewhere; the room light would be different there and different results would be obtained. Light Emitting Diodes (LEDs) were the next option because they possess a linear relationship between forward current and luminous output intensity. Since the light level needed was an unknown, a selection of LEDs were chosen and a circuit was designed to have the LEDs operate in the full on position. If none of the diodes produced a sufficient luminous intensity, they can be arrayed to create a designated output intensity. A diode selection array was designed, and built, to determine the best diode for illuminating the well plates (Figure 20 LED schematic.). The array and viewing stage was covered with a black cloth to completely block out all other light except the light produced by the LED array.

The LEDs ranged in peak wavelength and light intensity value (Table 1) and they were cycled through using the two different cameras (CCD-400, CCD-500) while the irises of the cameras were adjusted to give the best resolution. The yellow green diode emitting 0.10 μW in combination with the CCD-400 camera gave the best resolution in checking various well plates filled with cells in various stages of development. The LEDs were of the encapsulated type, and the output intensities were determined using a photometer with a flat spectral response to all wavelengths involved, so the measurements are accurate in relation to one another.

5.2. CONCEPT VALIDATION

Using the fiber optic sensing system, a change in refractive index of the cells over time was observed (Figure 21 HuTK- cells lifetime plotted with index of refraction., Figure 22 VERO cells lifetime plotted using index of refraction). This revealed that refractive index of the cells changed over time. Since this was the case, is it possible to use this phenomena to change the characteristics of a light beam passing through the cells?

Using a step density filter, the individual fibers were checked to determine their individual response to increasing optical densities (Figure 23, Figure 24, Figure 25, Figure 26, Figure 27, Figure 28, Figure 29). The straight line in these curves represent a least square fit, and the slightly curved lines are the experimental measurements. All the fibers exhibited a characteristic increase in intensity between the optical densities of 0.3 - 0.7. This could be attributed to imperfections in the step density filter. If the step density filter's film thickness' are not exact according to the optical density of the material, this effect will be seen in actual readings. Fibers 3, 4, and 7 exhibited the most linear response. The differences in individual optical fiber's response to optical densities probably arises from aberrations occurring during the polishing process. To account for these differences, the seven optical fiber measurements were averaged. This should serve to not only "smooth" out the data, but it will provide a more macroscopic picture of the well.

The impact of the meniscus of the cell culture media inside the wells of the 96 well plates on the transmittance was another reason for averaging the data points of all seven fibers. Fiber 7, which is in the center of the well, always had a higher reading than the rest of the fibers in the well. Meniscus lensing was also observed when the image was viewed under the light microscope. After realizing all these factors, measurement of pure media in the well was taken. After averaging, the readings were very similar (Table 2).

A bubble formed in the media and connected to the underside of the microtiter lid. It resulted in a marked increase in the transmittance of the light (Table 3). The bubble appeared to capture the light and act as a lens when viewed through the optical fiber, producing results similar to those observed for the condensation effect. This is entirely possible because it is known that a thin film will cause a maxima on light passing through it based upon equations 21 and 22.

Condensation on the underside of the microtiter lid increased the light transmittance intensity (Table 4). Since the exact amount of condensation on the underside of the top plate protecting the wells could not be controlled, the top plate was removed to take measurements because different condensation amounts could overrule the actual impact the cells could have on the transmitted light. Removing the top plate had one major drawback in that it possibly exposed the cells to contamination; therefore, after the reading was taken of the 96 well plate, it was discarded.

It was also seen that if extreme care was not taken in the collection of the data, significant error could be induced (Table 5 Error impact on transmittance produced by misalignment of the well plate.). It is very easy to misalign the masking plate and change the reading by physical means instead of reading the impact from the cellular environment. Unfortunately, the Fresnel Fiberscope is currently a "crude" device in comparison to the degree of sensitivity needed to actually pursue this work to the level desired, but it is a good starting point.

It was seen that a higher cellular density monolayer produced a "lensing" affect. The results from a 96 well plate containing VERO cells are shown in Table 6, Table 7, Table 8, and Table 9. The wells with a higher seed density show a higher transmittance. This is not entirely surprising since the same effect is observed on the light microscope. The cells were measured one hour after being placed inside the wells.

A developing monolayer of cells were studied since the preliminary work indicated the feasibility of following cellular development using the Fresnel Fiberscope. The development of VERO and CV1 cells impact on transmittance were followed to determine the impact of the cellular processes in light transmittance through the sample. The results are not conclusive since not enough data has been accumulated to completely characterize the cellular systems, but early work revealed some surprising cellular characteristics.

Figure 31 and Figure 32 are graphs of the effect of a developing VERO monolayer on light transmittance. The straight line is the average media value. The interesting feature of these graphs is that the higher seed density wells actually allowed more light to pass. The cells appear to have a lensing effect. As time progresses, the wells become somewhat similar in their impact of the light passing through the wells. The reason light transmittance through the well C5 on 22 February dropped significantly was because the cells started dying and turning dark (Figure 39). This reduced the amount of light that was allowed to pass through the well. Figure 33 shows the images of the endfaces of the fiber optic bundle during data collection. Figures 34 - 39 are the microscope images taken to correlate to the seed density to data measured using the NIH software.

When CV1 cells were measured the opposite effect was seen. The higher seed density blocked more light. This is probably due to the fibrous nature of the cells actually causing a “sheet” effect of the light trying to pass through the well. Again the cells exhibited the similar characteristics after a few days (Figure 40, Figure 41). The drastic decrease in transmittance in well C1 is due the plate being misaligned during the reading. Misalignment is one of the main contributors to measurement error. Figure 42 shows the images of the endfaces of the fiber optic bundle during data collection, and Figures 43 - 48 are the microscope images taken to correlate to the seed density to data measured using the NIH software.

5.3. CONCLUSIONS

The Fresnel Fiberscope is designed to accommodate future development needs. Originally the camera was mounted at a fixed point with respect to the well plate. This did not give the option of increasing the camera’s field of view. Currently it is still mounted at a fixed point until all the correlations are established, but it is placed on an optical stand with an adjustable z axis. This will allow the freedom to let the camera drop back from the well plate to increase the field of view. In this manner the entire 96 well plate can be monitored using one camera.

The camera chosen is a GBC CCD-400. It is a high resolution (400 lines) 0.03 lux camera with a minimum of 10 shades of gray scale. The CCD-400 was chosen over a more sensitive, 0.01 lux (CCD-500), camera because the CCD-500 lux was too sensitive. The lux is the camera's reaction to incident luminance, a smaller lux means the camera needs a smaller incident luminance to produce a picture. Both cameras use an adjustable lens with an adjustable iris to control input light intensity. The iris on the CCD-500 was 3/4 closed to achieve the correct sensitivity over a step density plate. The CCD-400 was able to have the iris fully opened. This eliminated possible diffraction effects shadowing the images near the edge of the iris.

When the system was used to capture images, the changes in light intensity were seen visually, but a method was needed to exactly determine the slight differences in light intensity. If the idea was to measure cellular impacts on the transmission properties of light, it was doubtful that the naked eye could distinguish the differences. A software program[11] was found that could be adapted to correlate light transmittance to an actual value. The version used was for a Macintosh Power PC. Images were captured on an IBM PC using a frame grabber (ALL-IN-WONDER by ATI Technologies), saved to a ZIP drive, and transported to the Macintosh for analysis. The PC version of the software program was not used because some of the functions do not work properly, and an external, commercial program is needed to emulate the program on the PC. Since money was an issue, the images were analyzed in the computer lab of the Center for Molecular Medicine and Infectious Diseases (CMMID), at Virginia Tech, on a Macintosh Power PC model 9500/200. After the images were analyzed with NIH Image, the output data was placed into an Excel (5.0) file. The Excel file was used to compile a graph of intensity versus index of refraction. A step density filter (Edmund Scientific - part number D32,599) was used as a standard to establish a correlation between individual fiber transmittances to different optical densities.

A top view of the viewing plate is illustrated in Figure 30. The idea behind the three viewing points, and their physical location, is to manually cover a series of cell culture densities. It is currently very difficult to cover the entire bottom of the 96 well plate because of the machining cost involved in fabricating a proper masking plate. By choosing the configuration illustrated in Figure 30, the 96 well plate containing the cells can be moved, from left to right, and readings can be taken in a serial fashion (i.e. A1, A3, A5, C1, C3, C5).

The refractive index changes of cellular systems were monitored using a fiber optic sensing system. The results showed a cyclical effect over the lifetime of the cellular environment. Although this path was not followed to a great length of research, it did show promise in point sensing of cellular environments. The data collected was used mainly to support the point that morphological changes of cellular lifetimes could affect refractive indices, thus validating the basic concept.

The information gained from the fiber optic sensing system was used as a stepping stone to investigate the design and construction of a device that would monitor cellular processes using changes in refractive indices to influence transmittance of light passing through the cellular environment. Our idea was discovered independently, although it was realized afterward that a similar idea had already come to fruition.[1] The University of California Lawrence Livermore National Laboratory, in collaboration with Tufts University, constructed an optical fiber imaging sensor that monitored the fluorescence of a solution to measure pH.

The "Fresnel Fiberscope" device constructed is able to view changes in optical density very well, as seen in the calibration graphs. The correlation of cellular processes to changes in transmittance will take much time and refinement of the instrument, but the basic premise is solid. Different cellular densities showed a marked affect on the transmittance of light through the sample. The device possesses the ability to be scaled to a desired image capturing size by changing the bundle dimensions of the optical fibers. The camera can also be used to capture a wide field of view and collect a tremendous amount of data in one frame.

The condensation effect could be removed by replacing the current stage with a heated one, or by mounting the viewing stage inside the incubator and running the optical fibers to a camera mounted safely outside the viewing environment. The effect of bubbles should also disappear, as they are usually incurred when handling the plates during observation. This ability to remotely sense cellular morphological activity is a tremendous benefit for monitoring the effect of hazardous viral strains on cells.

5.4. FUTURE DIRECTIONS

The future applications of the idea of the Fresnel Fiberscope are almost limitless. It is at the same stage as the Bonanni microscope of 1691 (Figure 3). It is very crude with respect to the possibility of resolution potential. Refinements could include a machining of the viewing stage to accurately align the 96 well plate and the mask. This would eliminate the current physical adjustments made while viewing the camera to obtain the best image. The author thinks this is the biggest contribution to measurement error. The fiber bundles could also be re-ground with greater precision, thereby removing the individual differences in the fibers observed during measurements. The size of the fibers used in the fiber bundle could be changed to increase, or decrease, the viewing diameter at the distal tip of the fibers. In this manner the device could be tailored to a specific size of cell in a cellular environment. Choosing an appropriate image analysis software would be a significant improvement, one such as IPLab Spectrum by Scanalytics (http://www.iplab.com/index.html) is made specifically for image analysis.

Potential future applications include zero gravity monitoring of cellular processes. Little is known about the effect of micro gravity on cellular processes; this device would allow in vitro observation on entire cellular systems. Strains of deadly viruses could be observed safely in space, or on the ground as the fibers could allow remote sensing of the environment. The data acquisition could also be automated, thus removing a great deal of human induced error, and the need for the tremendous amount of time currently incurred in data acquisition of cellular systems.

Miniaturization on the device is also possible. A microchip LED could be mounted on the top plate and a photodiode could be used to collect the information transmitted into the optical fiber. The device could be used in fields of toxicology, virology, immunology, and biology, to name a few. Since is impossible to view viruses with a light microscope, the cytopathic effect of a virus on a system could be observed, rather inexpensively, in laboratories around the world. A scanning electron microscope is needed to view viruses, and only an "after the fact" assessment can be made. With this device, a viral progression could be monitored while it occurred. This would tremendously increase the speed of research into the effect of viruses on cellular systems.

The cost of a Fresnel Fiberscope system, once it is fully developed, should be around the same price as a good light microscope. This would enable more scientists to study effects and processes currently only available to more "equipped" laboratories, allowing data access of cellular systems to a great deal of researchers on a limited budget. Since the data could be collected with a computer, it would also greatly facilitate information transfer via the Internet.

On a final note, the Fresnel Fiberscope is not the end all answer to cellular and virological monitoring. The early results show promise, but many refinements need to be made to establish concretely the correlation between the transmittance and the reason for the changes. If this device is developed, and improved, it could have the same impact on the biological community that fiber optics has had on the communications community.

6. TABLES

Table 1 Characteristics of the LEDs used in the Fresnel Fiberscope.

Light Emitting Diode	Peak wavelength	Irradiance at faceplate (W/cm^2)	Irradiance at experimental distance of 5 1/2”
Yellow Green	565 nm	64.1 μW	0.10 μW
Yellow Jumbo	590 nm	372 μW	44.3 μW
Orange Jumbo	620 nm	5.62 mW	250 μW
Bi-color Red	660 nm	4.33 mW	30.69 μW

Table 2 Determination of pure media effect on transmittance.

	Well Position	
Fiber Number	A3	Well A5
1	8051	7249
2	7599	7247
3	8249	8444
4	7290	6605
5	6758	7071
6	7817	7817
7	8374	8416
Average	7734	7550
	C1	C3
1	7550	7550
2	6695	6780
3	8402	8358
4	7275	7088
5	7364	7101
6	7994	7551
7	8457	8342
Average	7677	7539

Values are in pixels.

Table 3 Measurement of a bubble, in the media of VERO cells, effect on transmittance.

	Well Position		
	A1	A3	A5
Seed Density	100,000	1,000	1,000
Fiber Number			
1	6699	7560	5721
2	7182	8073	6063
3	8094	7635	7800
4	6897	6795	5313
5	6573	6312	4833
6	6726	8787	7062
7	8529	9480	9231
Average	7242	7806	6576

Values are in pixels.

Table 4 VERO cells; effect of condensation on transmittance.

	Well Position: A1	
Fiber Number	With Condensation	Without Condensation
1	9300	8850
2	7605	6984
3	7854	7257
4	5352	4674
5	8655	8076
6	6504	6135
7	7128	6342
Average	7485	6903

Values are in pixels.

Table 5 Error impact on transmittance produced by misalignment of the well plate.

	Well Position		
	A1	A3	A5
Seed Density	100,000	1,000	1,000
Fiber Number			
1	7773	8163	7614
2	6576	8349	7041
3	7809	6165	8097
4	6543	6537	6687
5	5562	5061	5427
6	7749	7398	7911
7	9048	8892	9237
Average	7293	7224	7431

Values are in pixels.

Table 6 VERO cells effect on transmittance.

	Well Position		
	C1	C3	C5
Seed Density	100,000	1,000	1,000
Fiber Number			
1	7572	6282	4785
2	5736	5190	3315
3	8529	8712	7485
4	7920	7149	6294
5	6711	6567	6519
6	7965	7425	7074
7	9801	9819	9969
Average	7749	7305	6492

Values are in pixels.

Data collected 2-3-98

Table 7 VERO cells effect on transmittance.

	Well Position		
	C1	C3	C5
Seed Density	100,000	1,000	1,000
Fiber Number			
1	7344	7461	5802
2	4368	6999	6600
3	8133	8451	4965
4	7290	6618	6414
5	7236	5160	6636
6	7563	8010	7980
7	9483	9285	9213
Average	7344	7425	6801

Values are in pixels.

Date collected 2-4-98

Table 8 VERO cells effect on transmittance.

	Well Position		
	A1	A3	A5
Seed Density	100,000	1,000	1,000
Fiber Number			
1	8586	8229	7506
2	8421	8061	6915
3	8895	8568	8739
4	7884	7788	8226
5	6585	6867	6012
6	8277	7752	8037
7	9897	9573	9741
Average	8364	8121	7881

Values are in pixels.

Date collected 2-5-98

Table 9 VERO cells effect on transmittance.

	Well Position		
	C1	C3	C5
Seed Density	100,000	1,000	1,000
Fiber Number			
1	7090	6483	6488
2	4490	5327	4817
3	7603	7752	6134
4	6974	7163	7012
5	6796	5373	5824
6	6942	6677	6861
7	8762	8816	8664
Average	6950	6799	6542

Values are in pixels.

Date collected 2-5-98

7. FIGURES

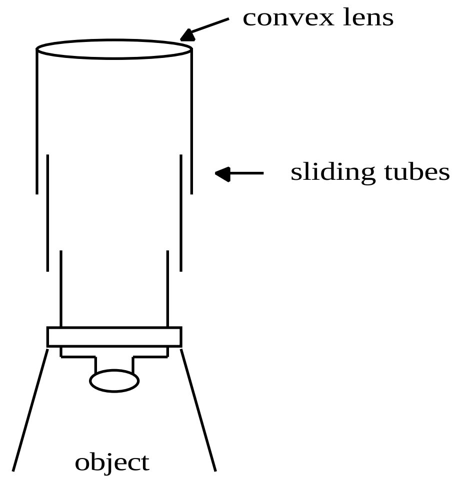

Figure 2 One of the earliest versions of the light microscope.

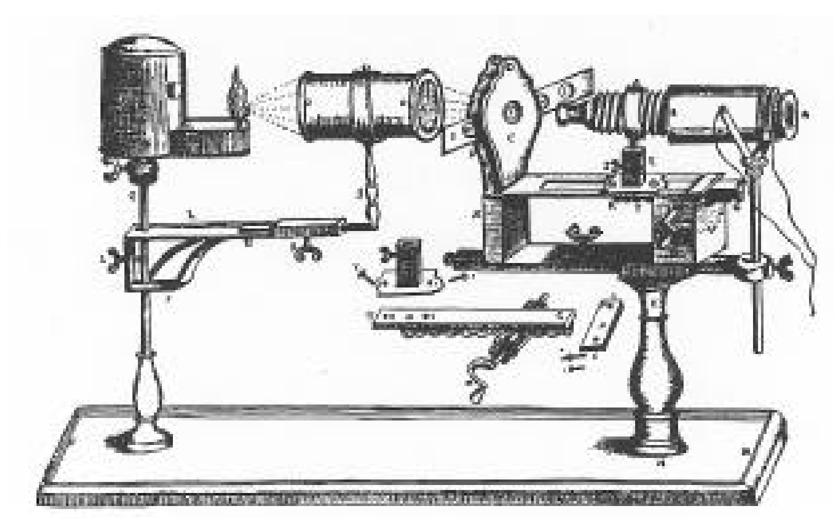

Figure 3[12] Early form of a commercial microscope. (Bonanni 1691)

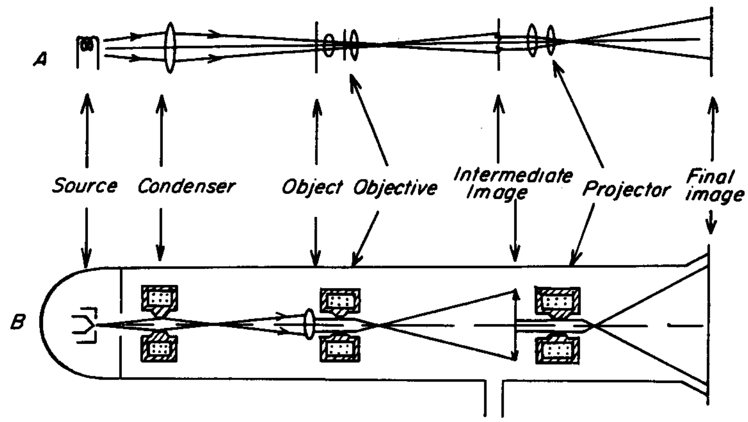

Figure 4[13] Comparison of a light and a scanning electron microscope.

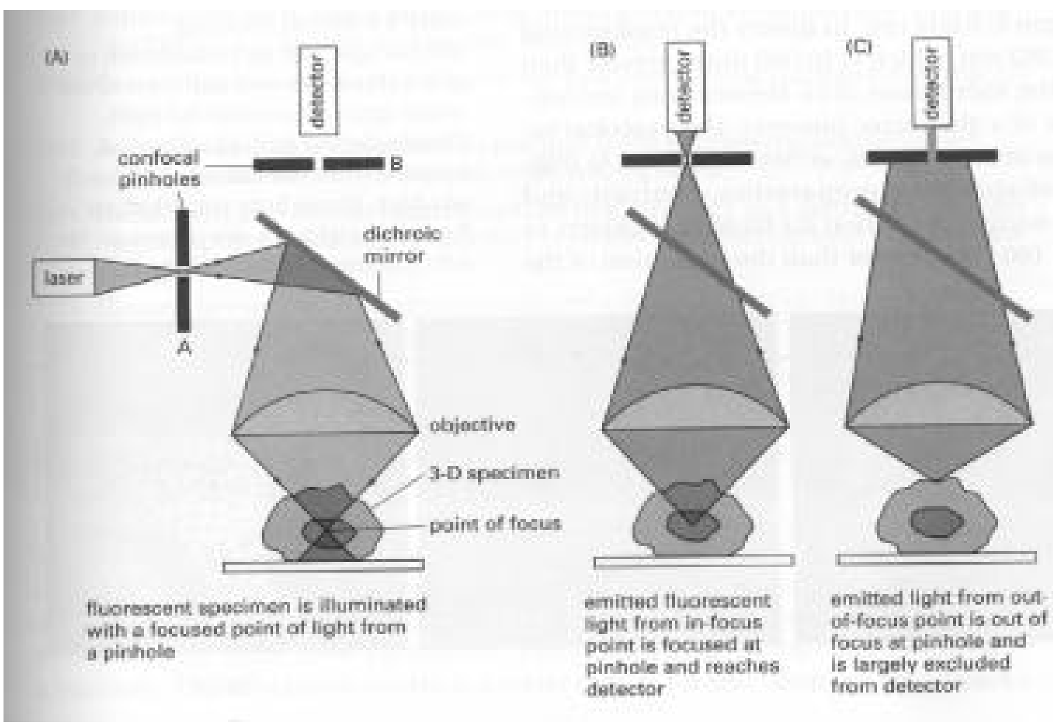

Figure 5[14] Con-Focal Scanning Microscope arrangement.

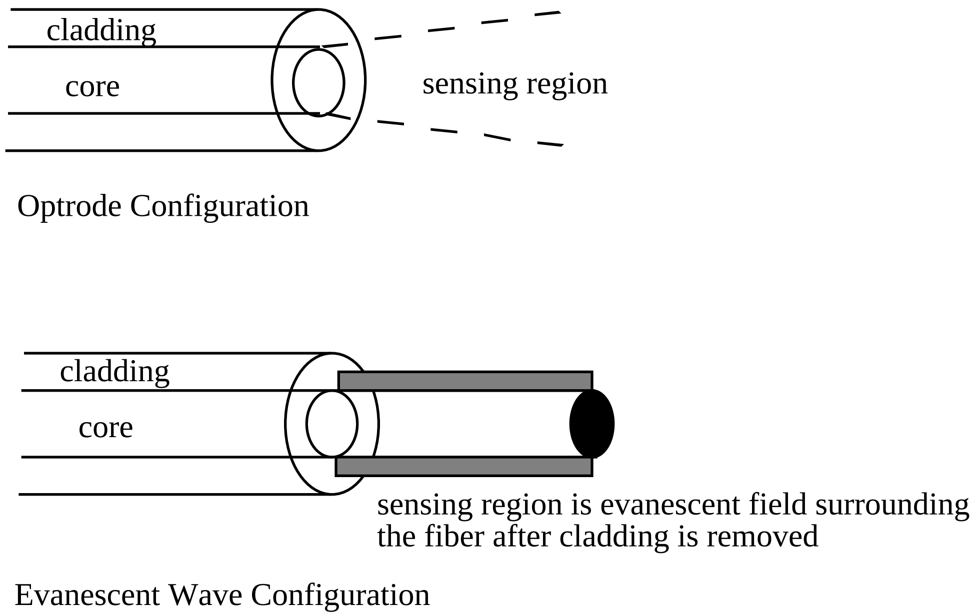

Figure 6[15] Optical field measurement configurations.

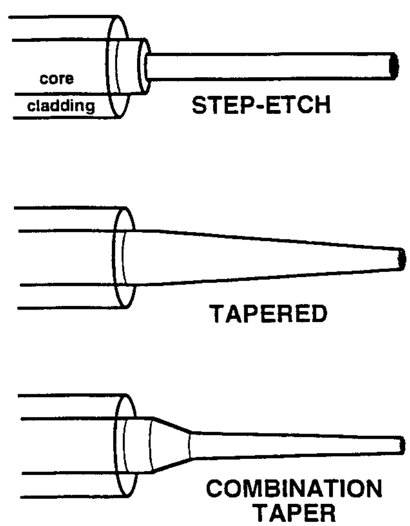

Figure 7[16] Geometries for evanescent field biosensors.

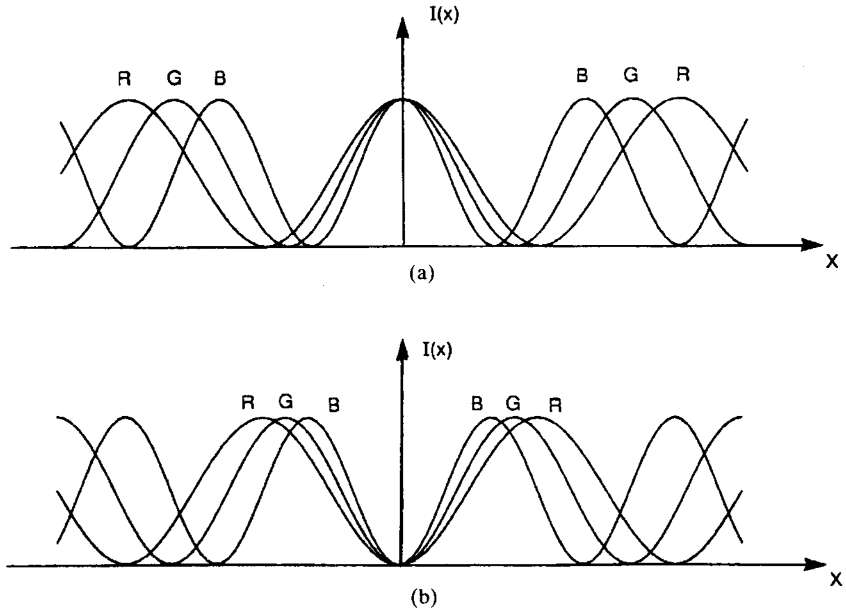

where I is intensity, x is distance, R is red, G is green, and B is blue.

Figure 8[17] Bright and dark fringes produced by optical phase differences.

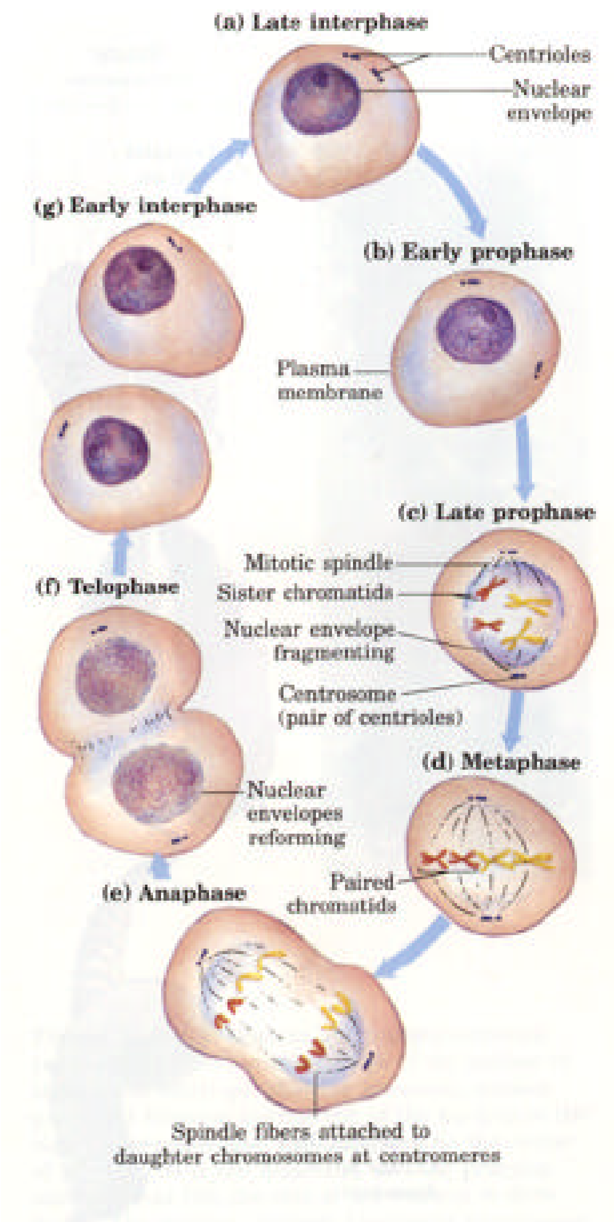

Figure 9[18] The process of cellular replication.

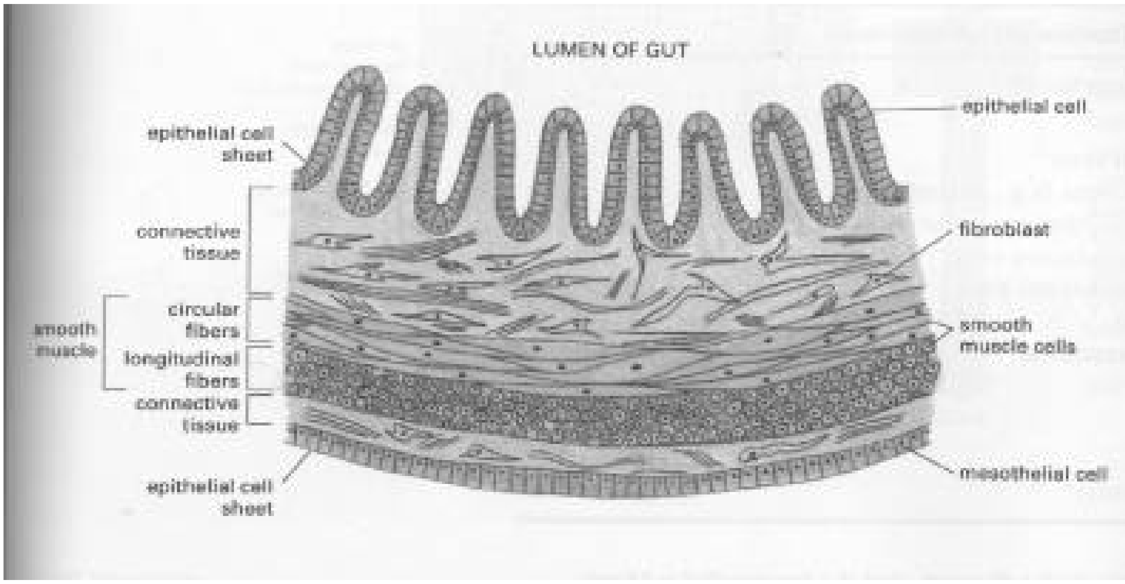

Figure 10[19] Lumen of Gut showing the difference between epithelial and fibroblast cells.

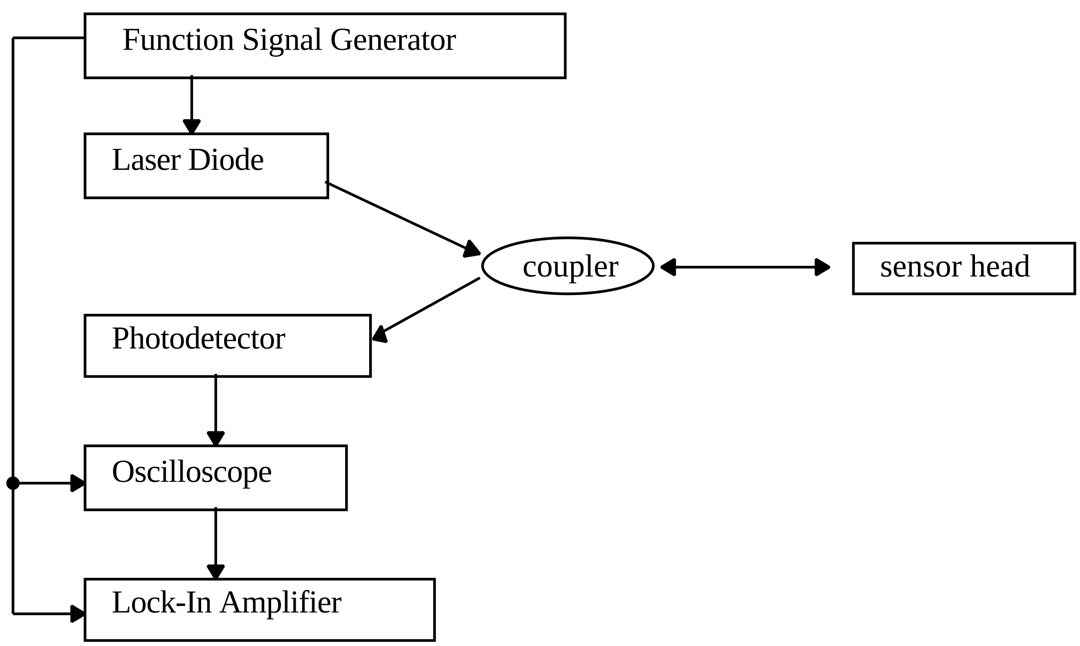

Figure 11 Block diagram for monitoring refractive index changes.

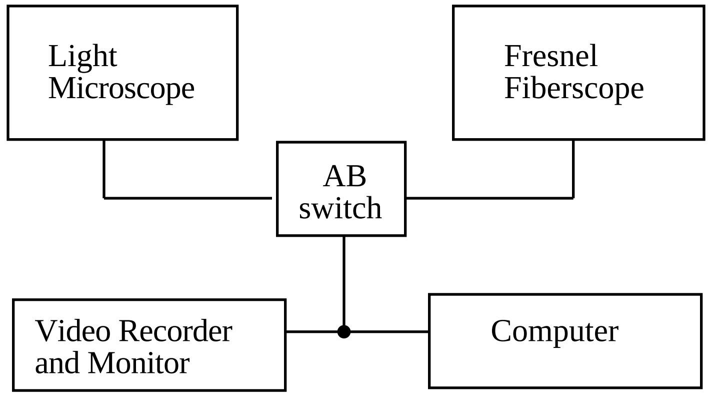

Figure 12 Block diagram of the Fresnel Fiberscope set-up.

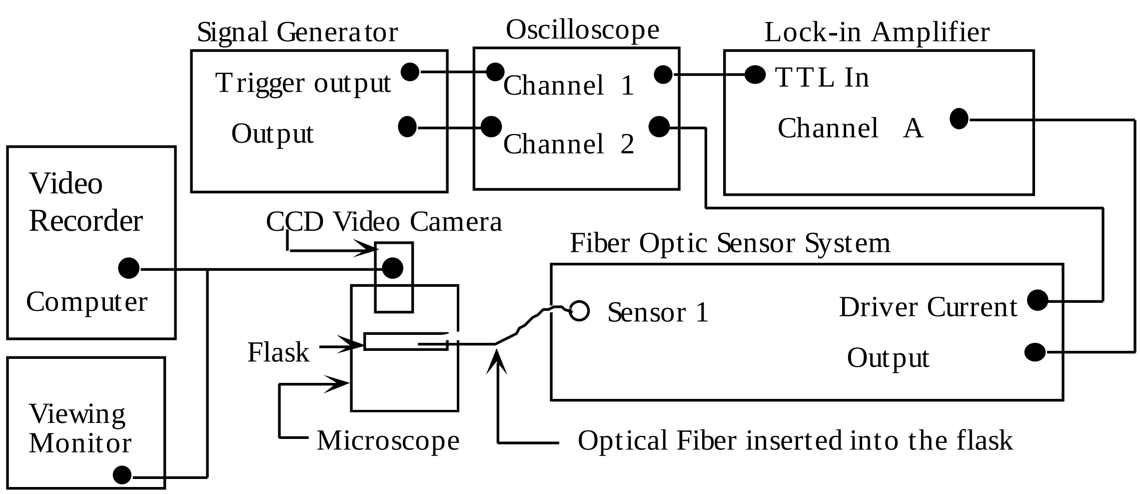

Figure 13 Experimental Set-Up for measuring refractive index changes using the single fiber method.

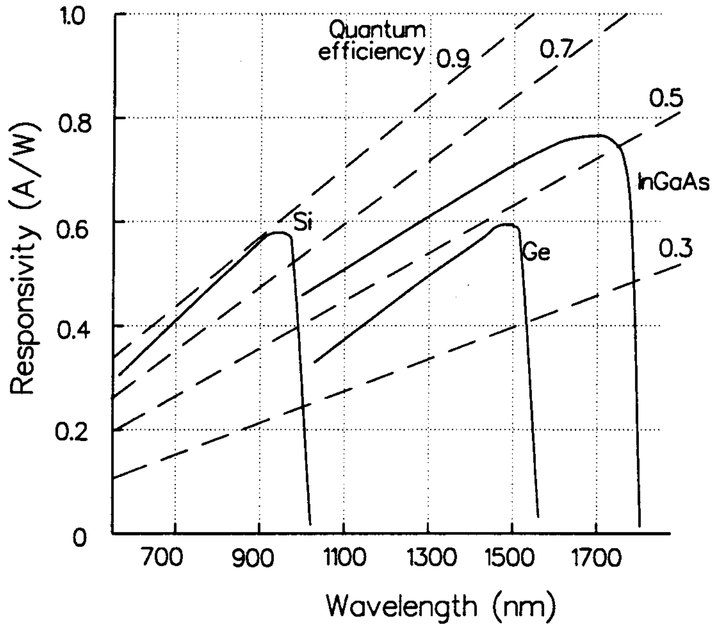

Figure 14[20] Responsivity vs. Wavelength for typical photodetector devices.

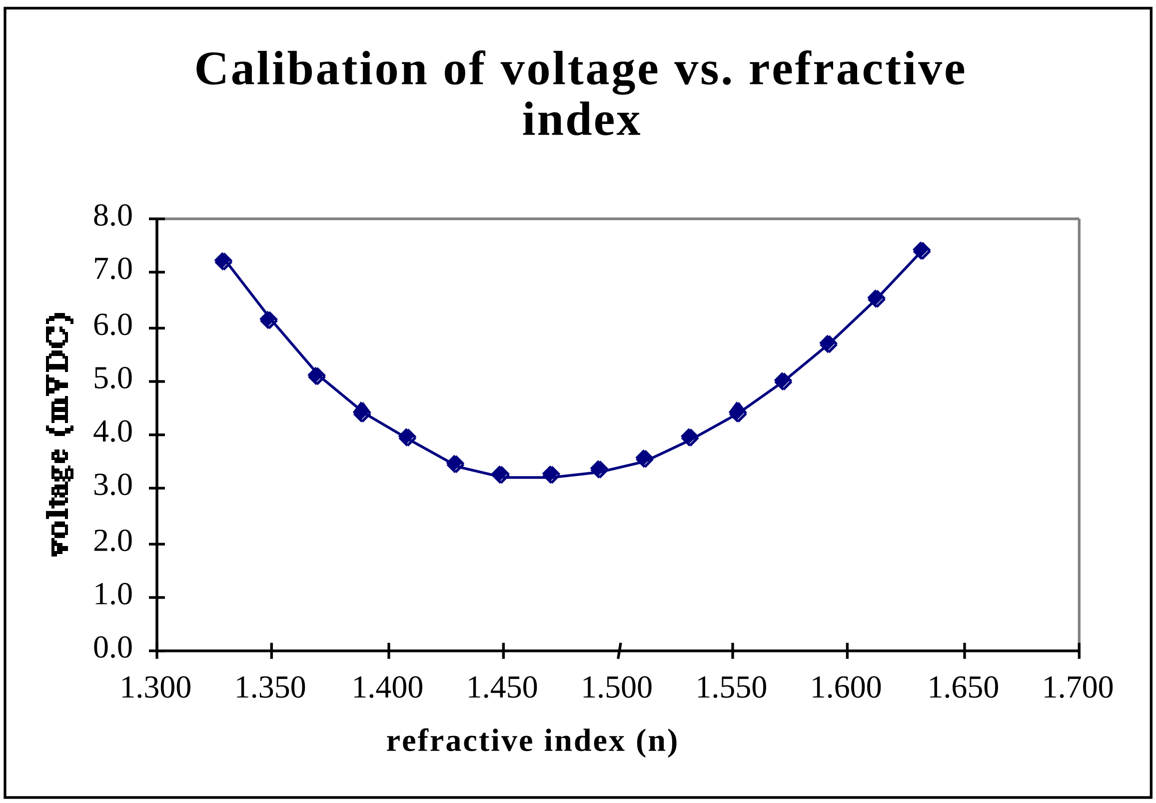

Figure 15 Refractive index vs. output voltage for a fiber sensor head calibration.

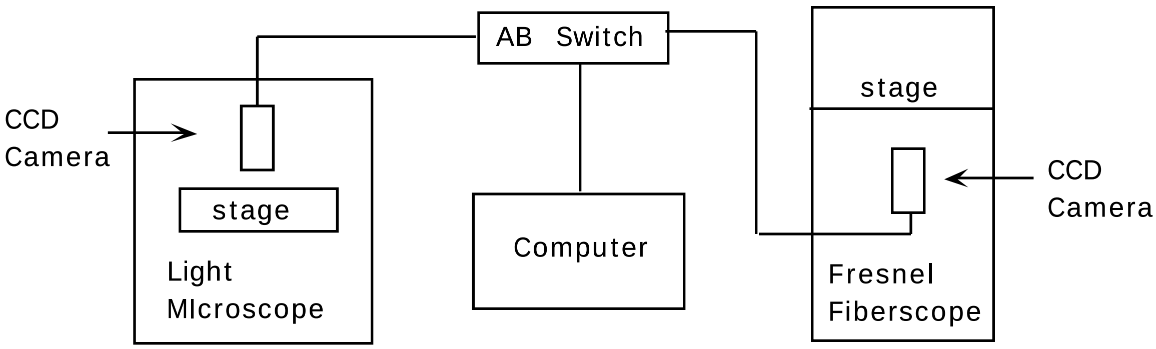

Figure 16 Experimental Set-up for the Fresnel Fiberscope.

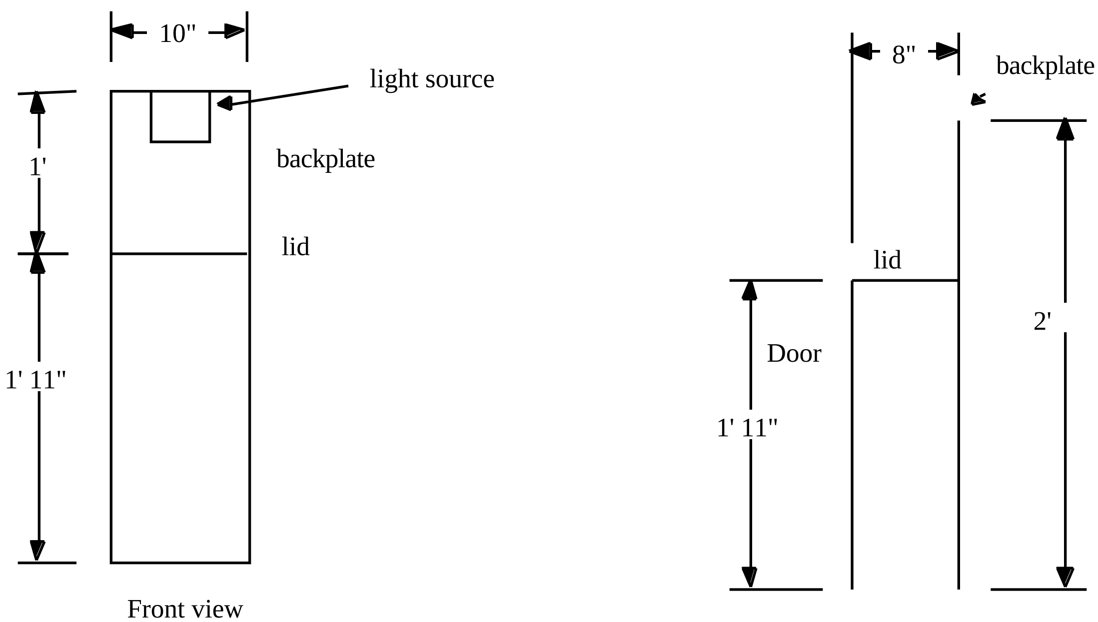

Figure 17 Drawing of the Fresnel Fiberscope box.

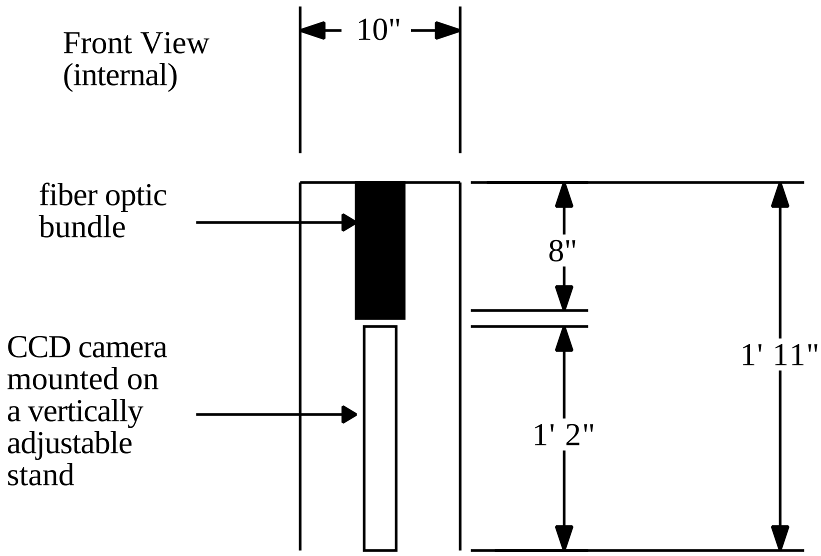

Figure 18 Internal picture of the Fresnel Fiberscope.

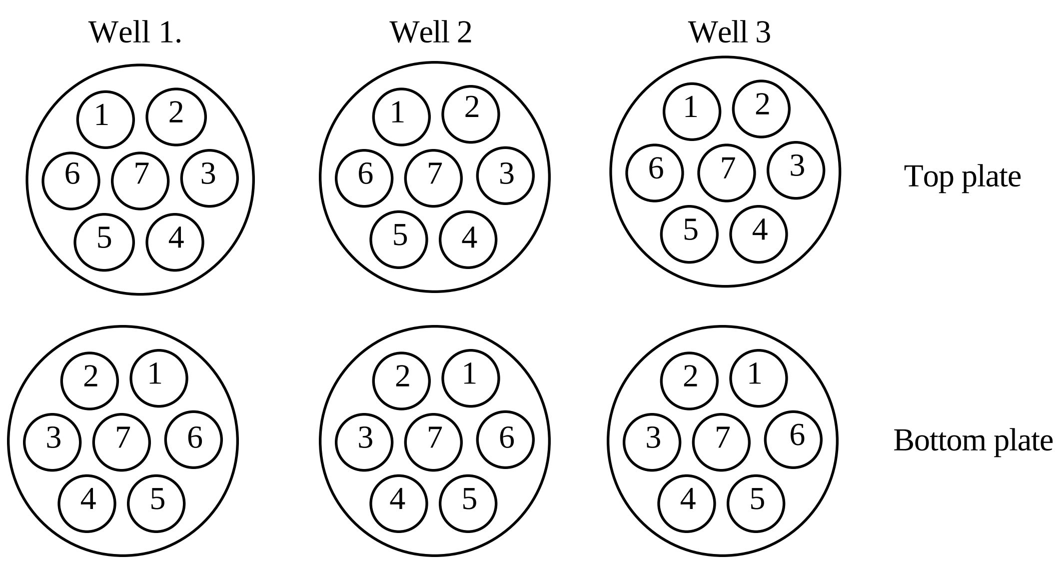

Figure 19 Correlation chart.

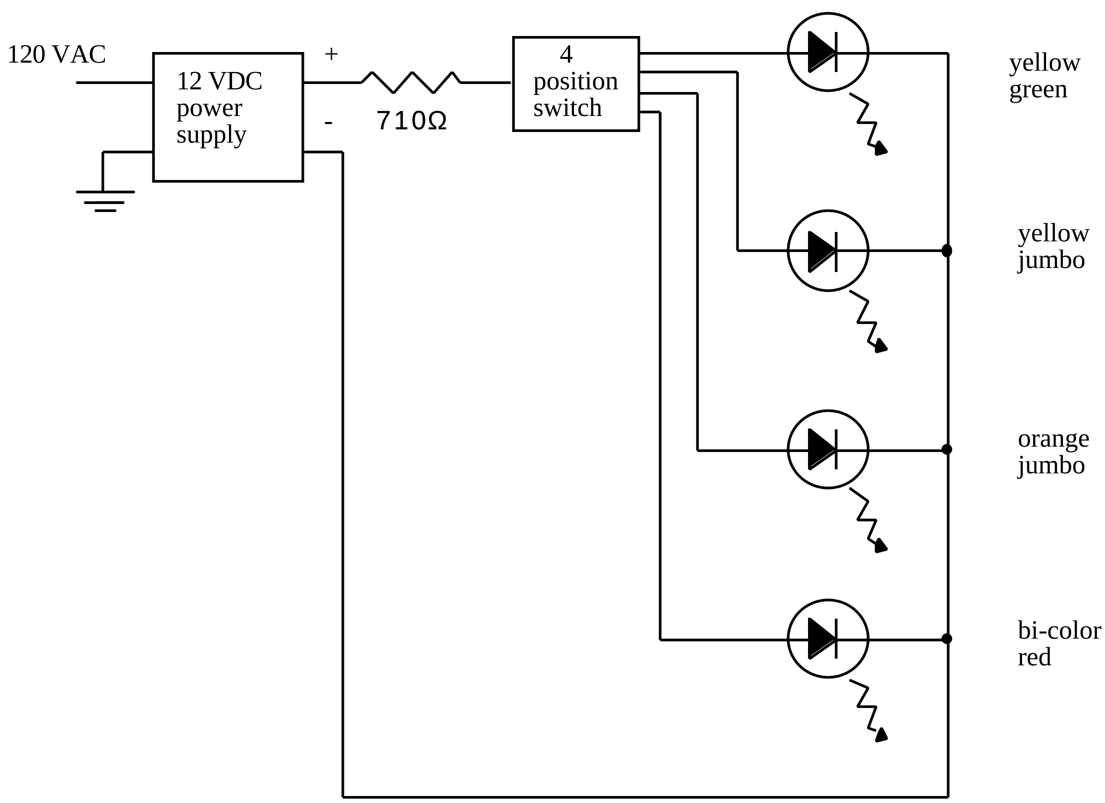

Figure 20 LED schematic.

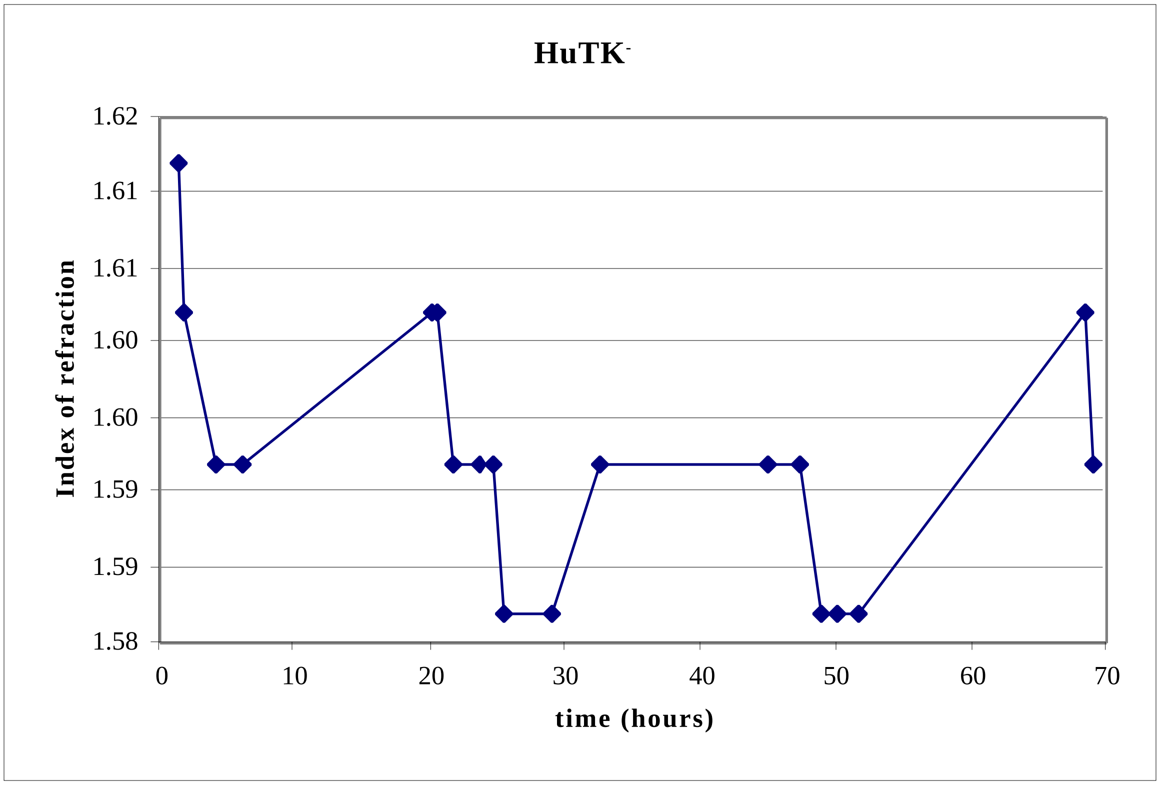

Figure 21 HuTK- cells lifetime plotted with index of refraction.

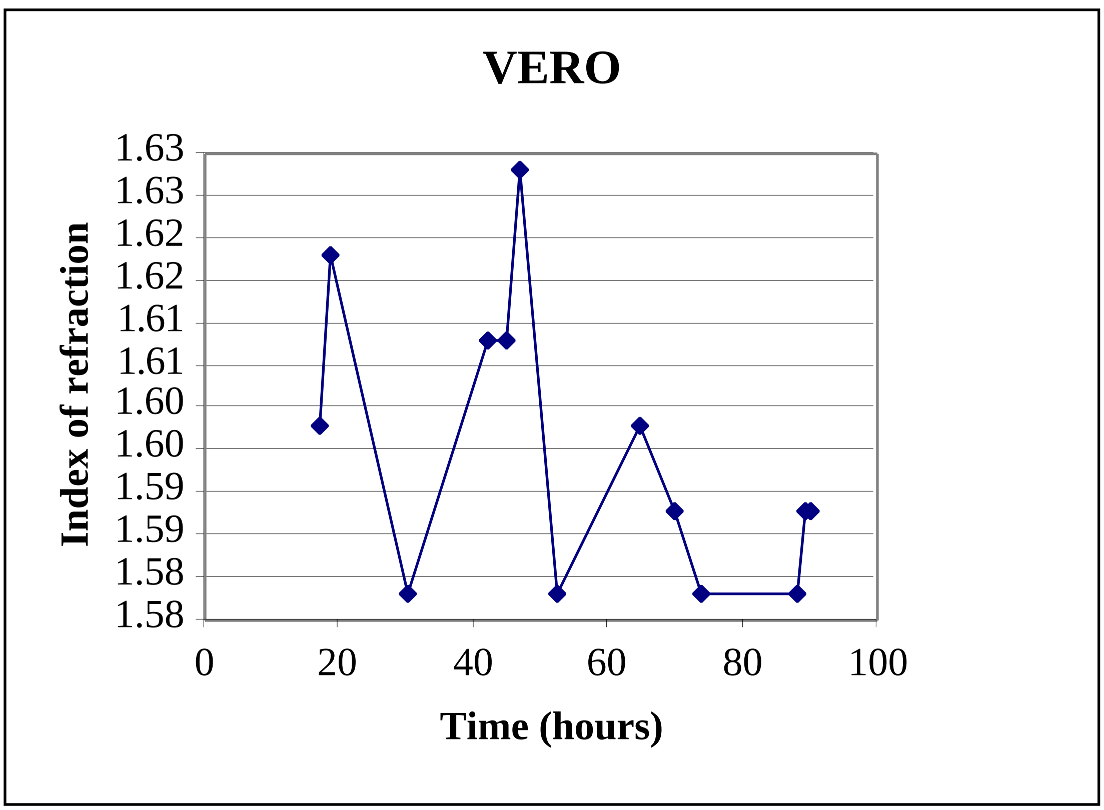

Figure 22 VERO cells lifetime plotted using index of refraction.

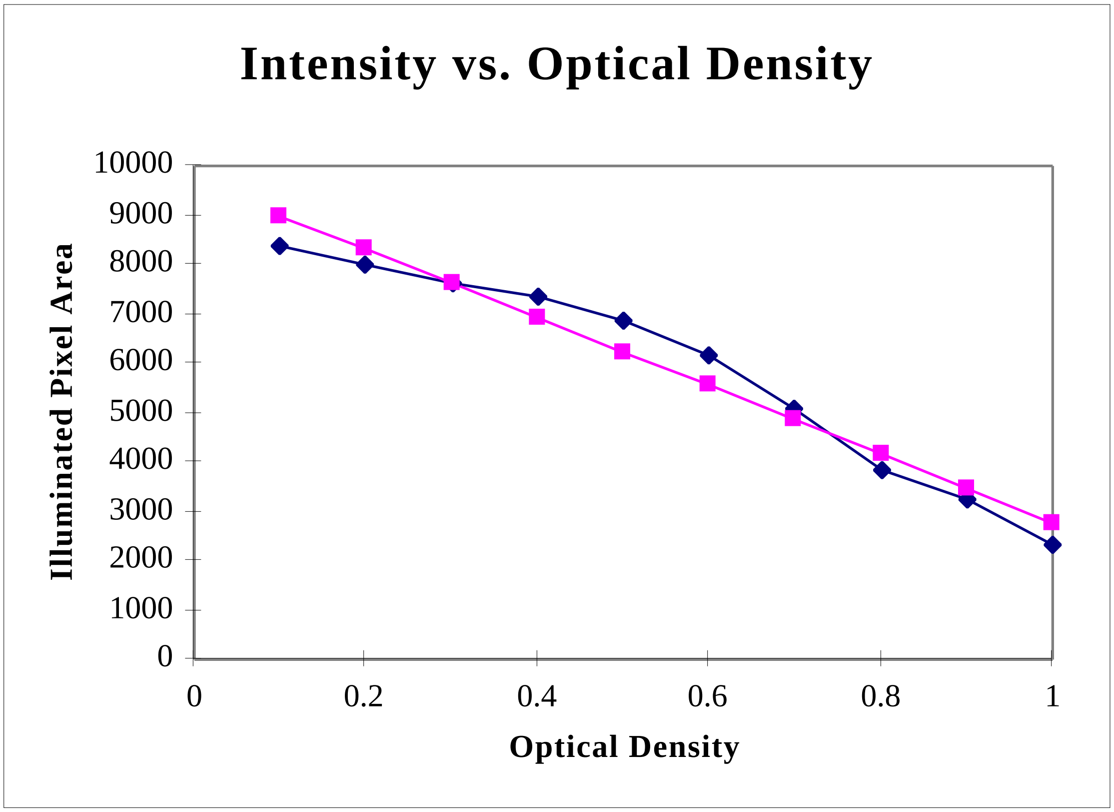

Figure 23 Fiber 1 calibration.

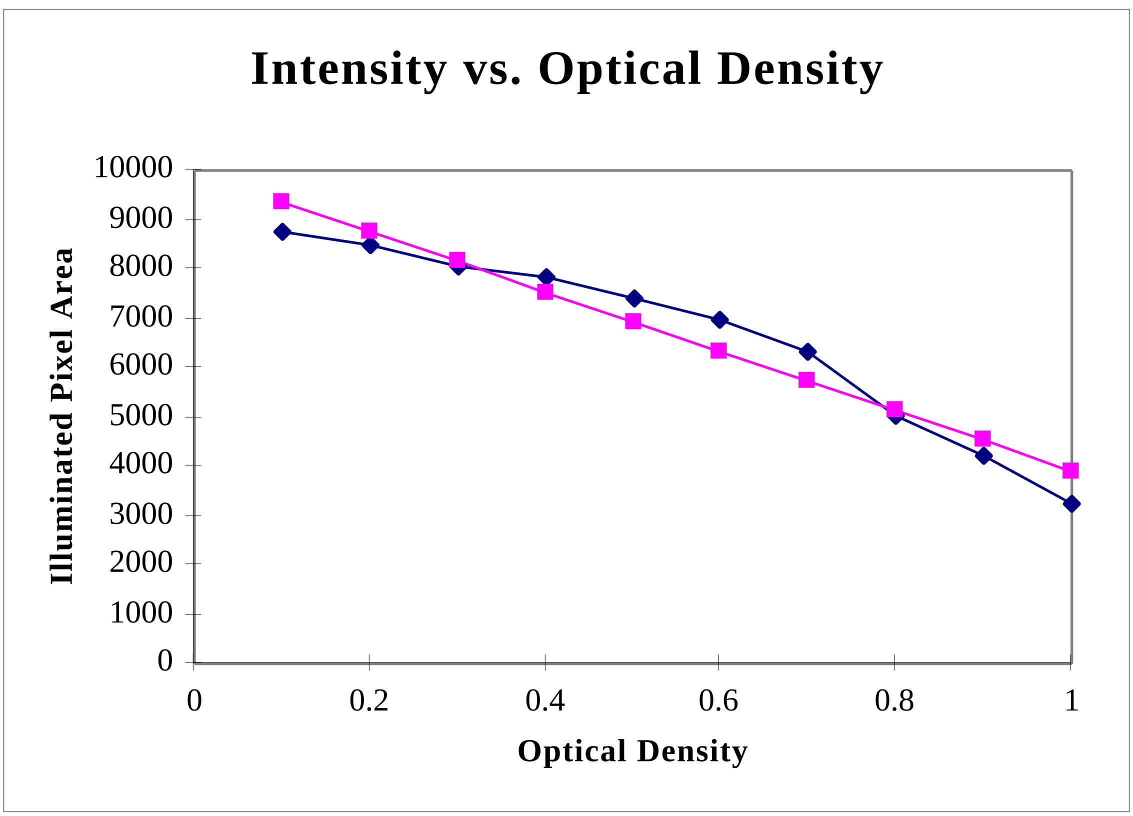

Figure 24 Fiber 2 calibration.

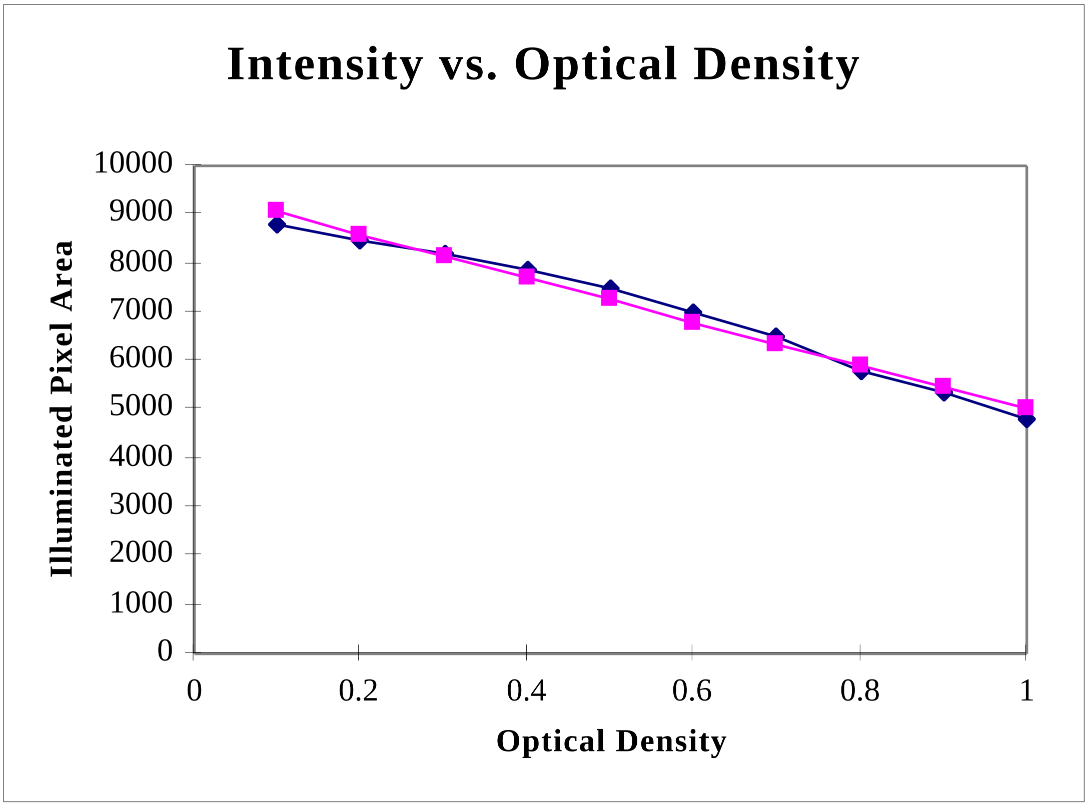

Figure 25 Fiber 3 calibration.

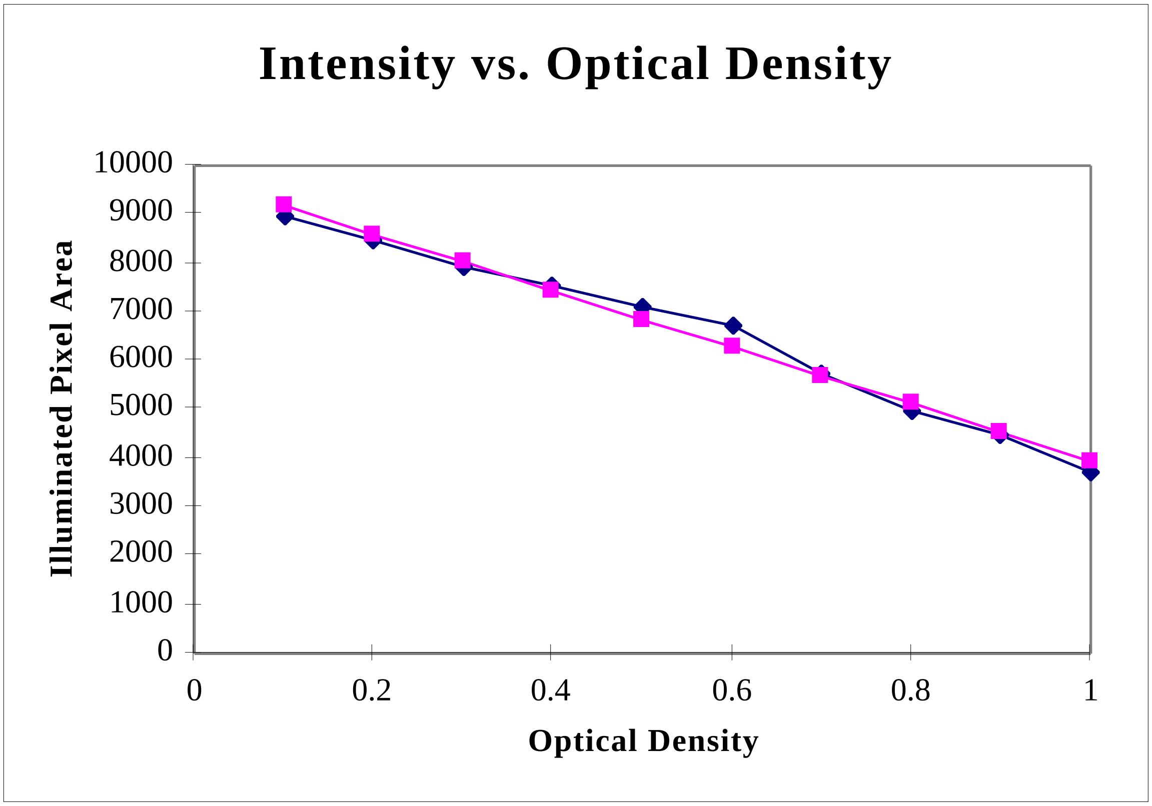

Figure 26 Fiber 4 calibration.

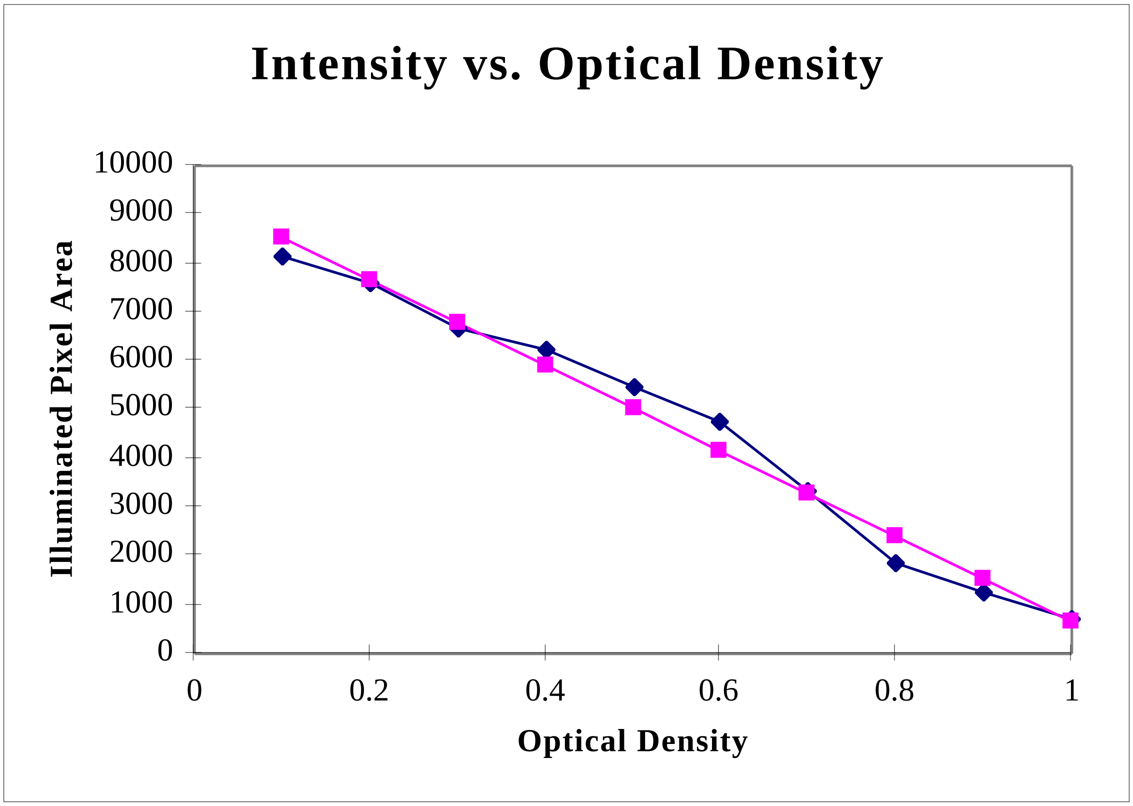

Figure 27 Fiber 5 calibration.

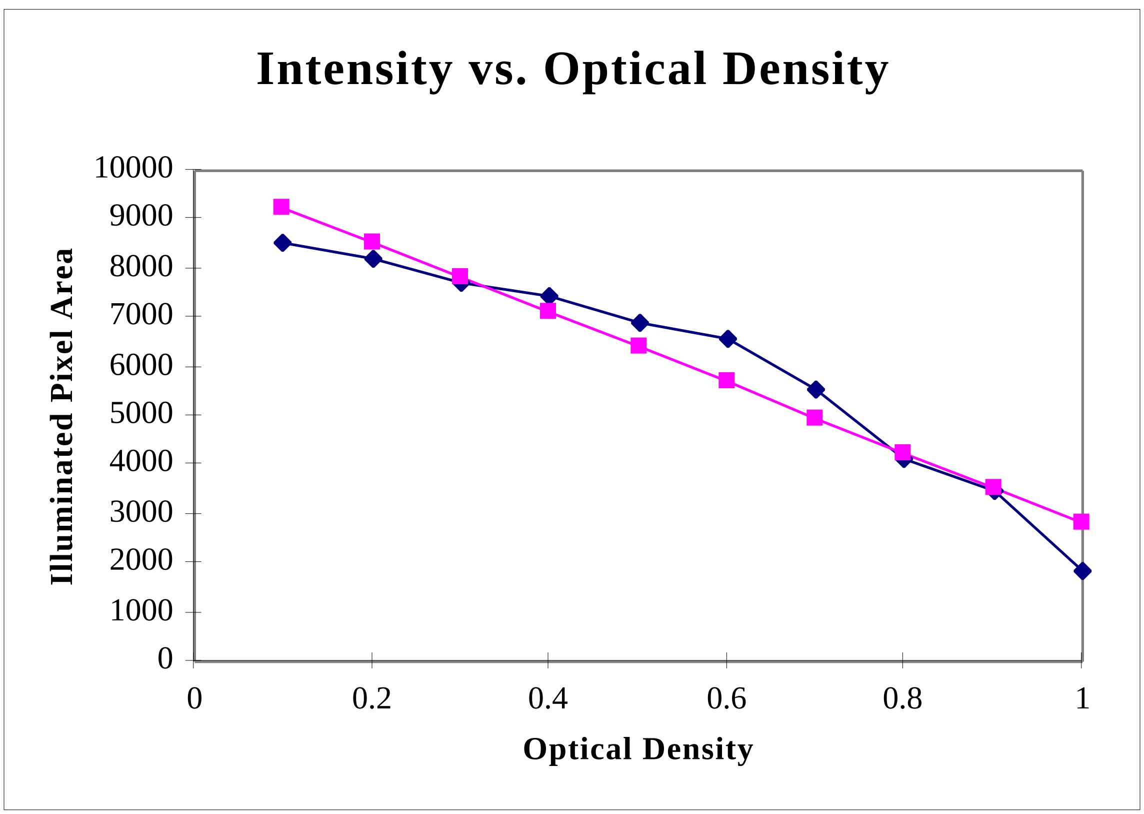

Figure 28 Fiber 6 calibration.

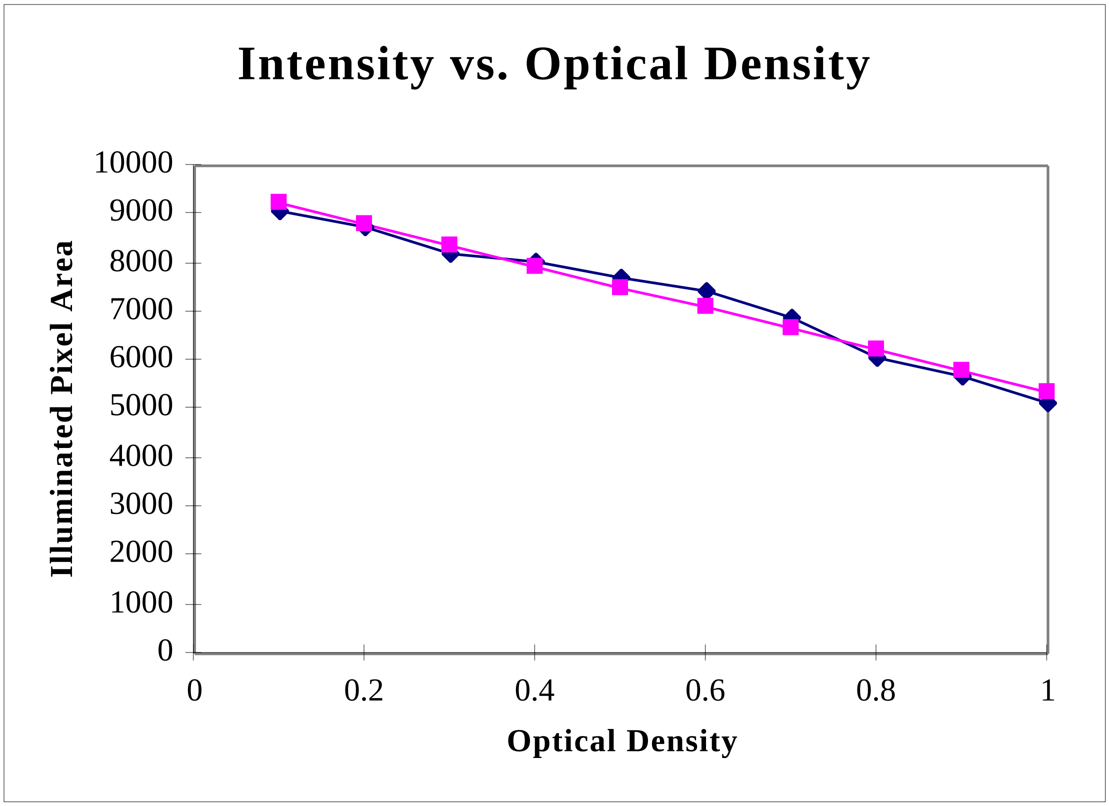

Figure 29 Fiber 7 calibration.

Top View of a 96 well plate. The black dots indicate fiber viewing positions

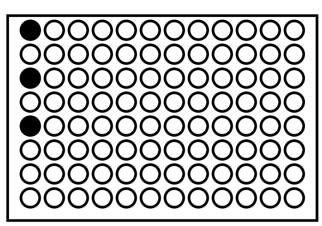

Figure 30 Top view of the viewing stage.

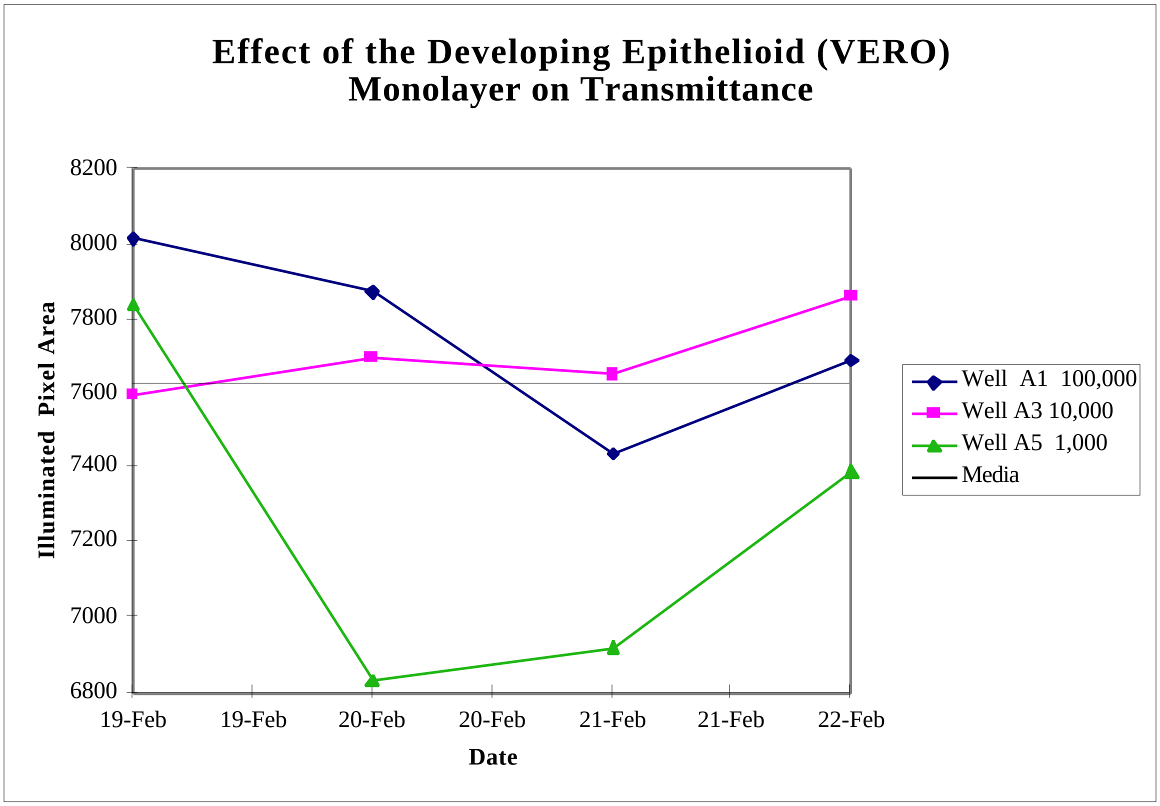

Figure 31 Effect of Developing VERO monolayer on Transmittance (A Wells).

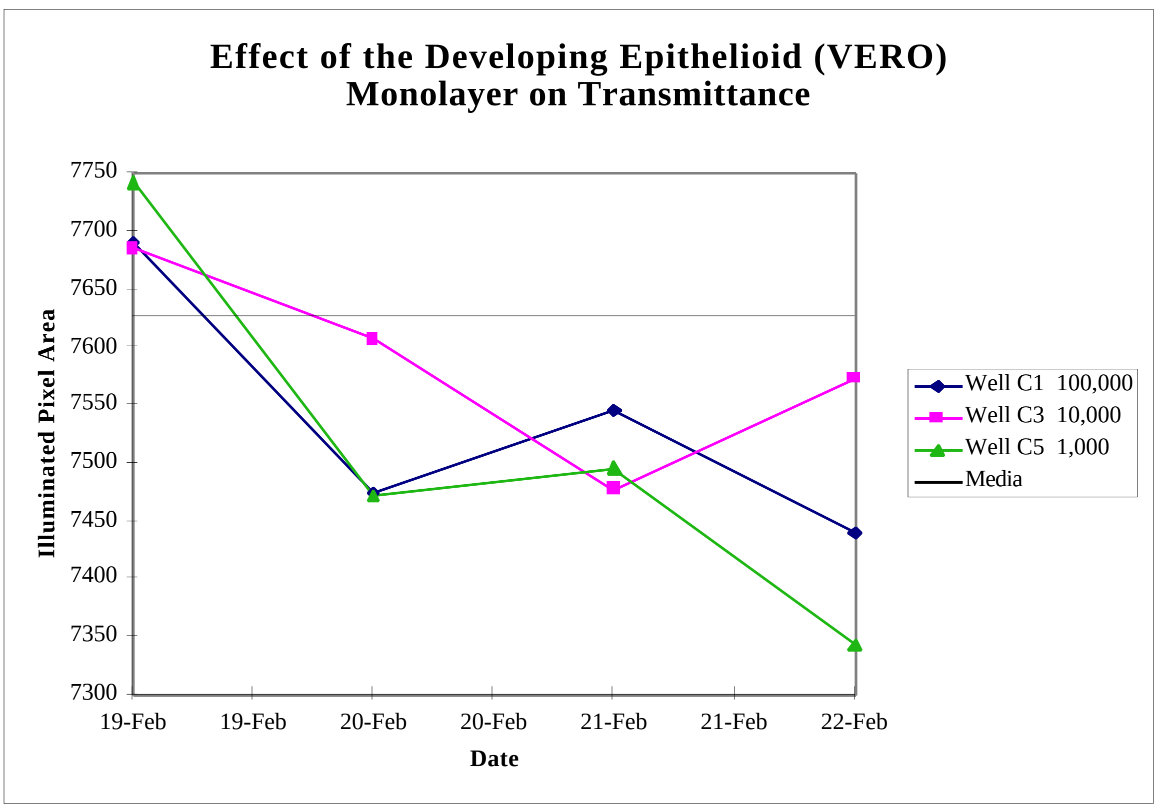

Figure 32 Effect of Developing VERO monolayer on Transmittance (C Wells).

Seed Density	C Wells	
100,000	10,000	1,000

19 Feb.

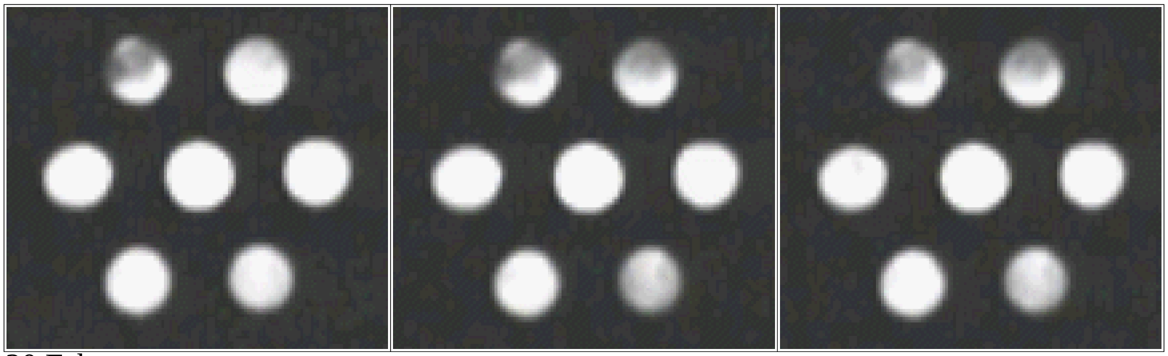

20 Feb.

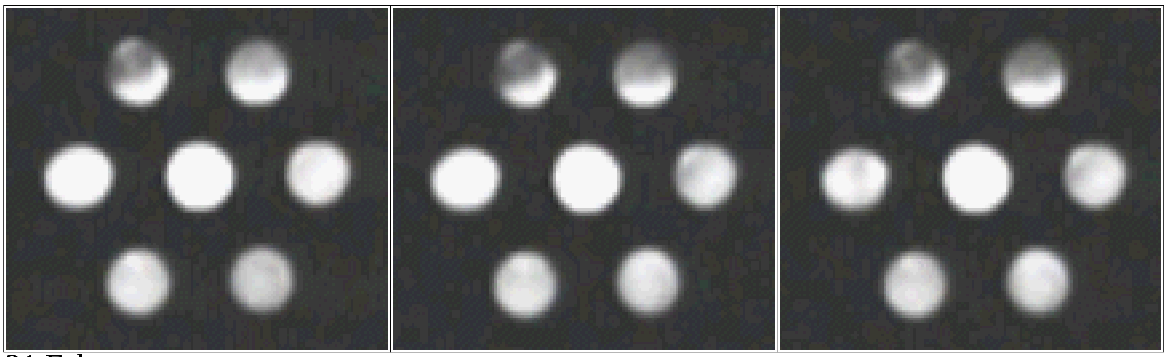

21 Feb.

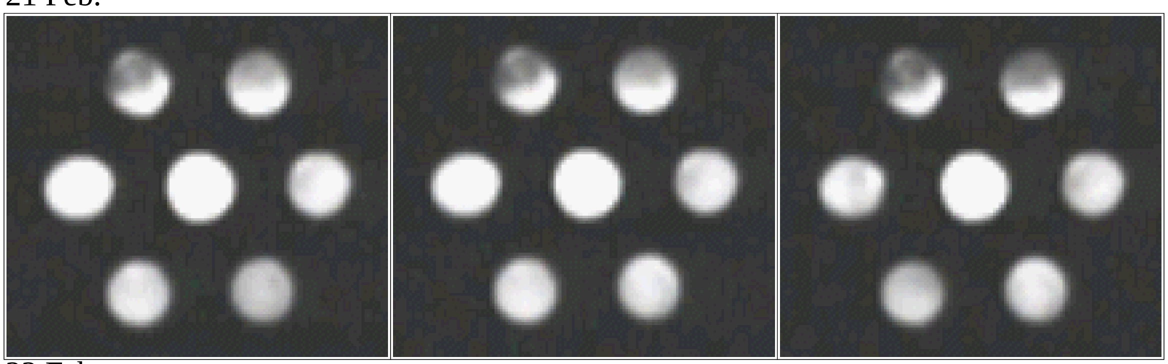

22 Feb.

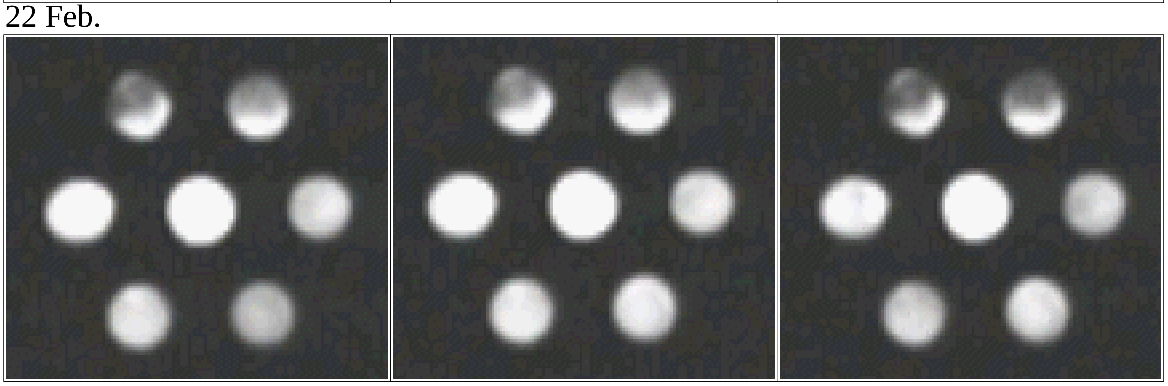

Figure 33 Images of Fiber Optic Bundle during data collection (VERO).

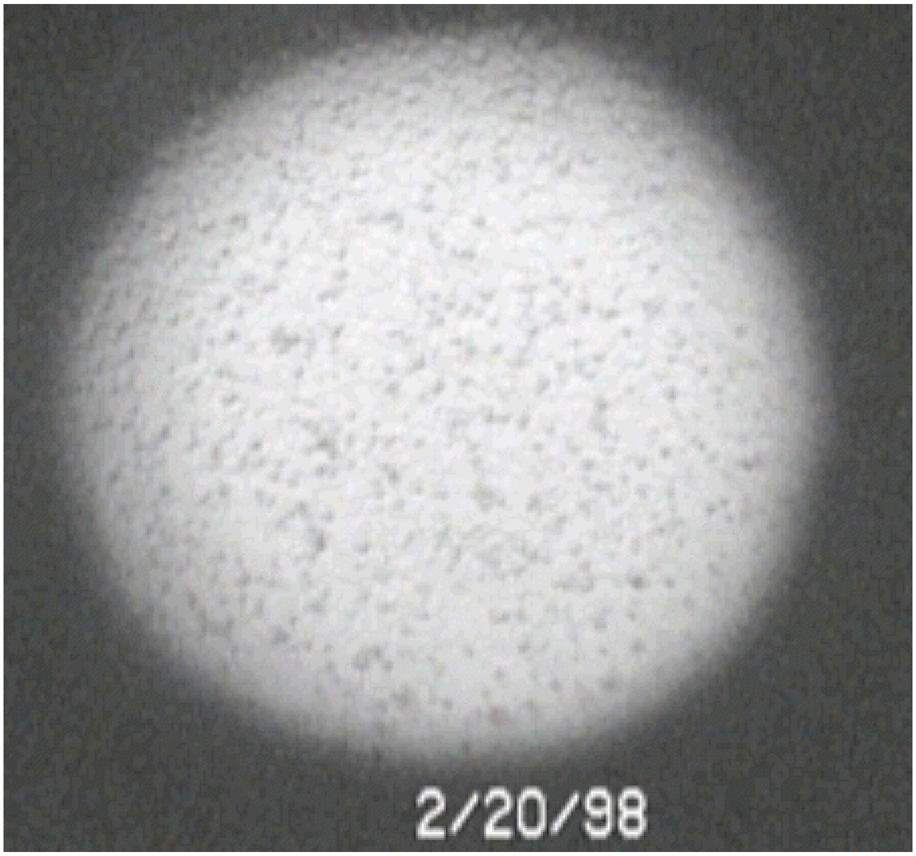

Figure 34 Microscope Image of 100,000 Seed Density (7690 pixels).

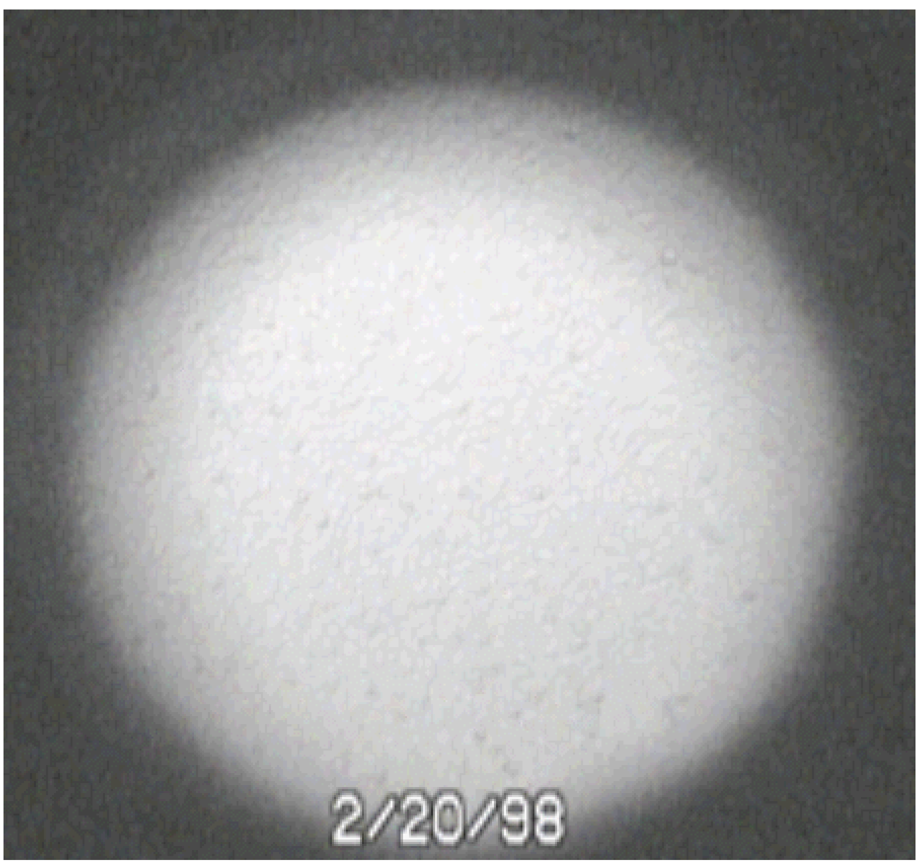

Figure 35 Microscope Image of 10,000 Seed Density (7686 pixels).

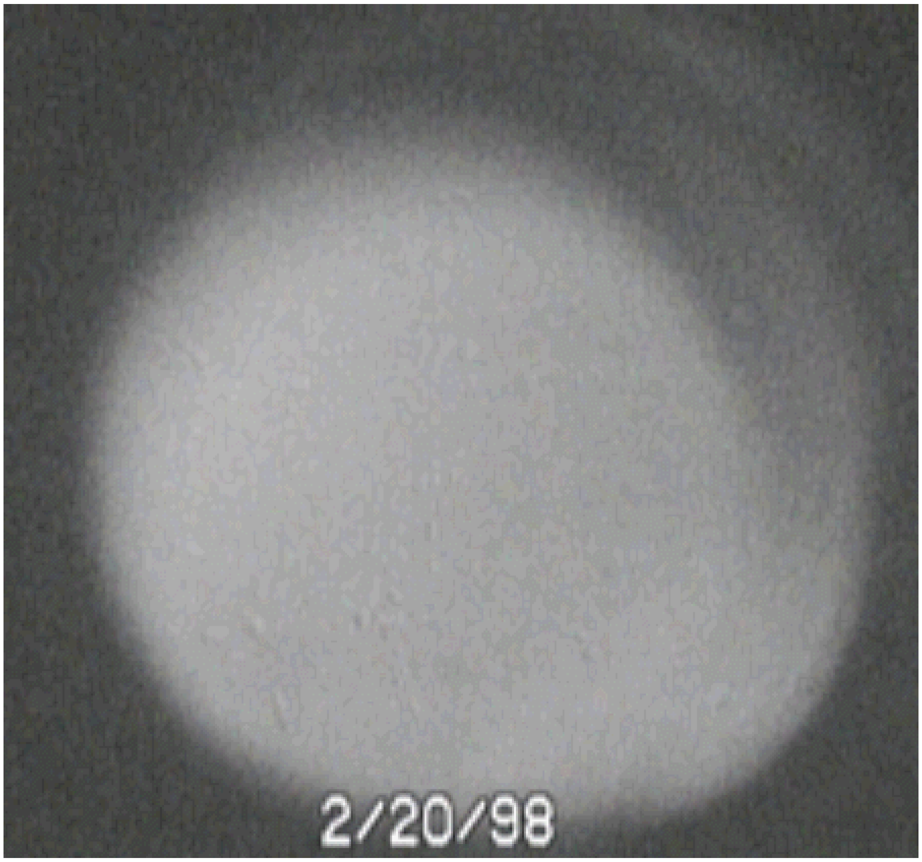

Figure 36 Microscope Image of 1,000 Seed Density (7744 pixels).

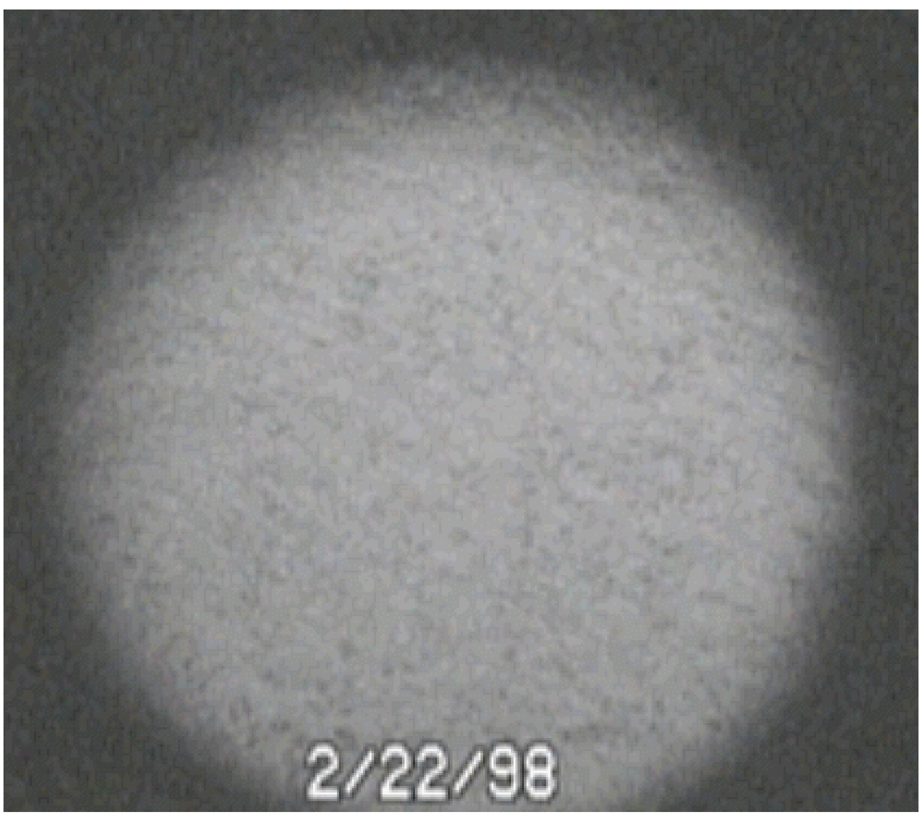

Figure 37 Microscope Image of 100,000 Seed Density (7439 pixels).

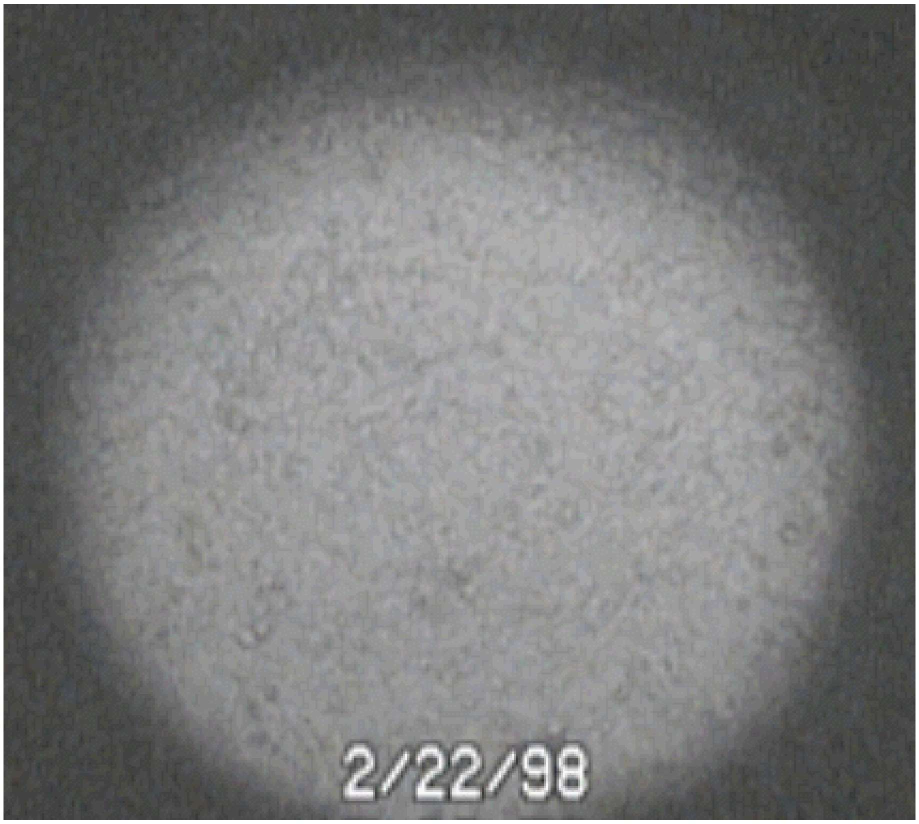

Figure 38 Microscope Image of 10,000 Seed Density (7572 pixels).

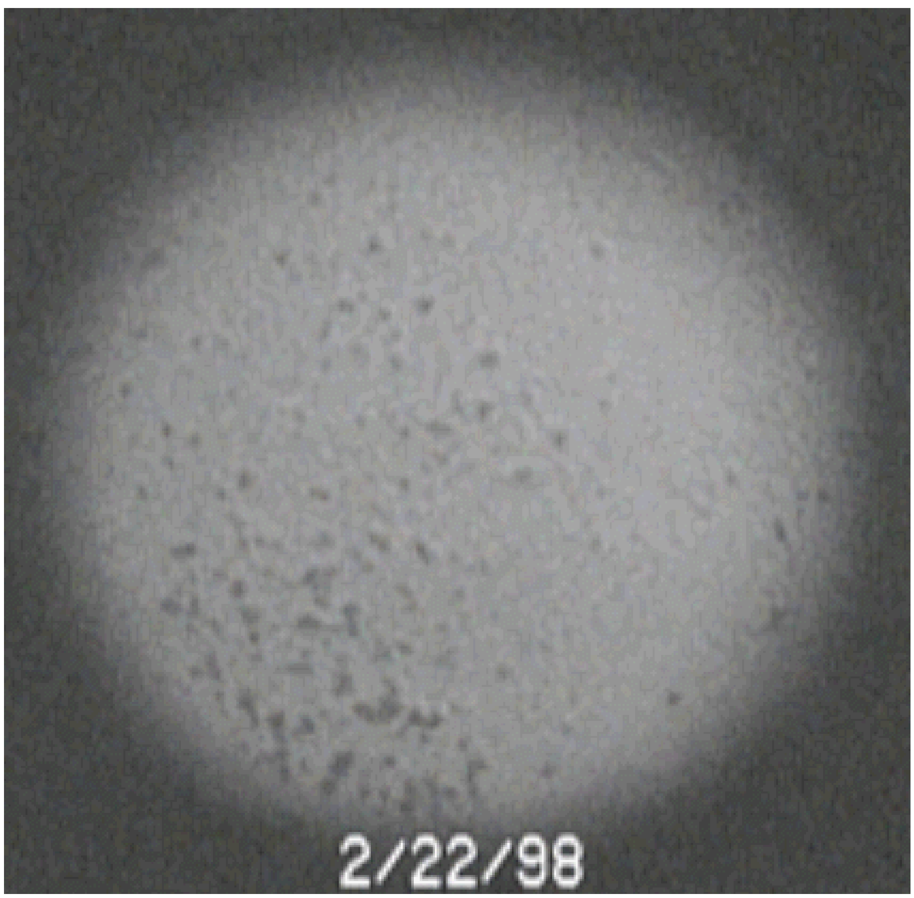

Figure 39 Microscope Image of 1,000 Seed Density (7342 pixels).

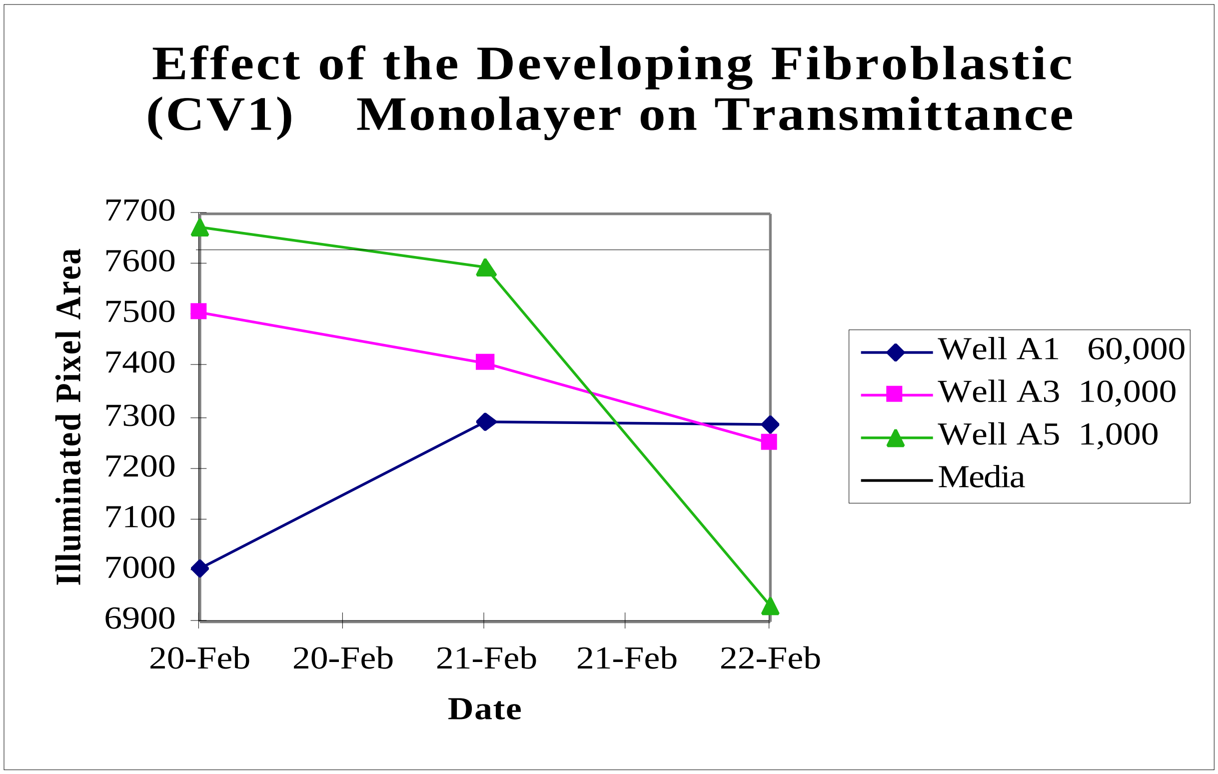

Figure 40 Effect of Developing CV1 monolayer on Transmittance (A Wells).

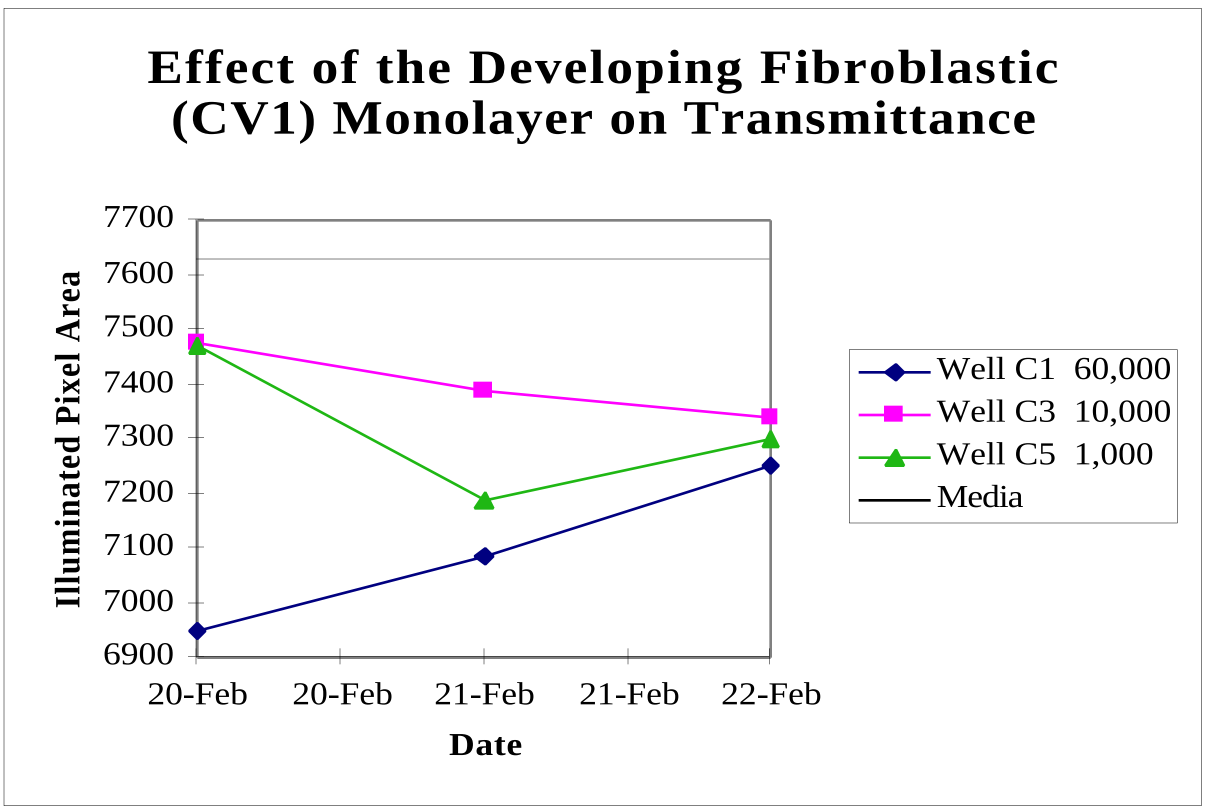

Figure 41 Effect of Developing CV1 monolayer on Transmittance (C Wells).

Seed Density	A Wells	
60,000	10,000	1,000

20 Feb.

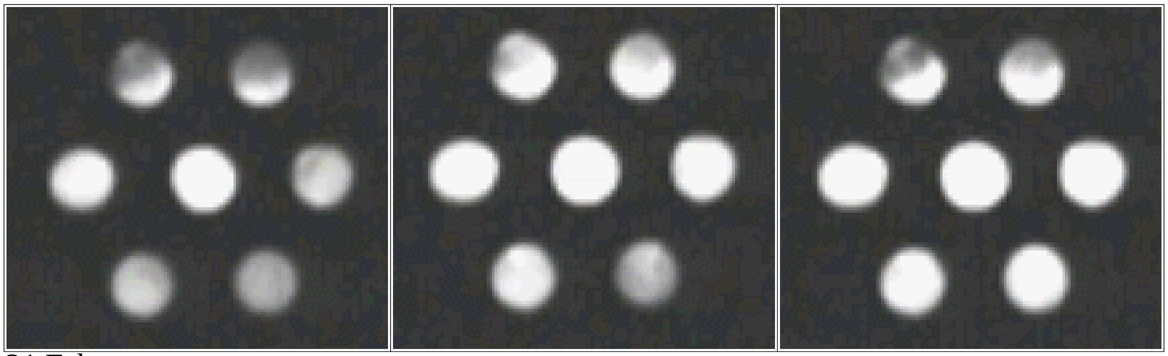

21 Feb.

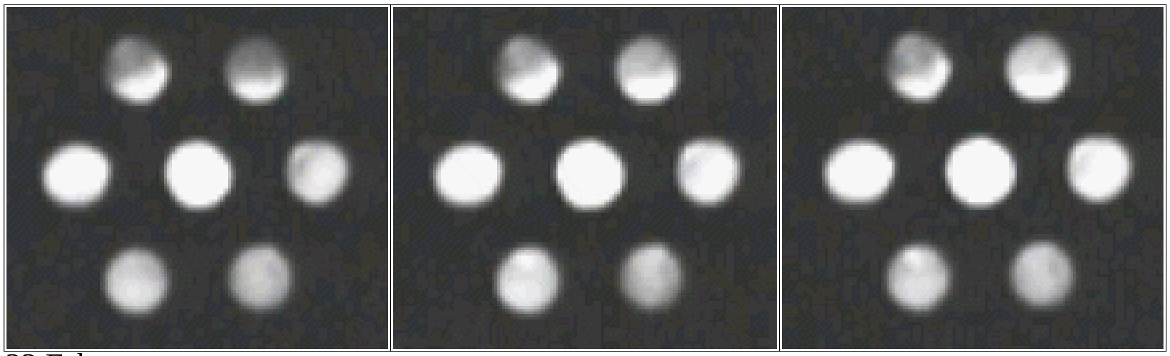

22 Feb.

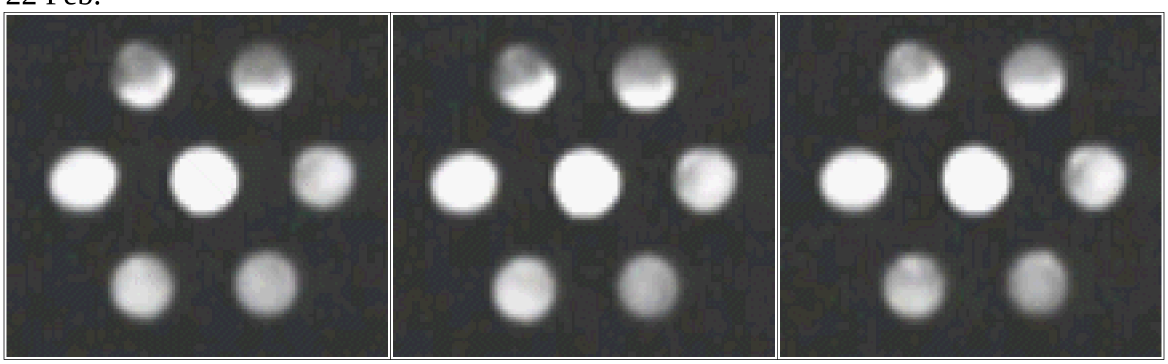

Figure 42 Images of Fiber Optic Bundle during data collection (CV1).

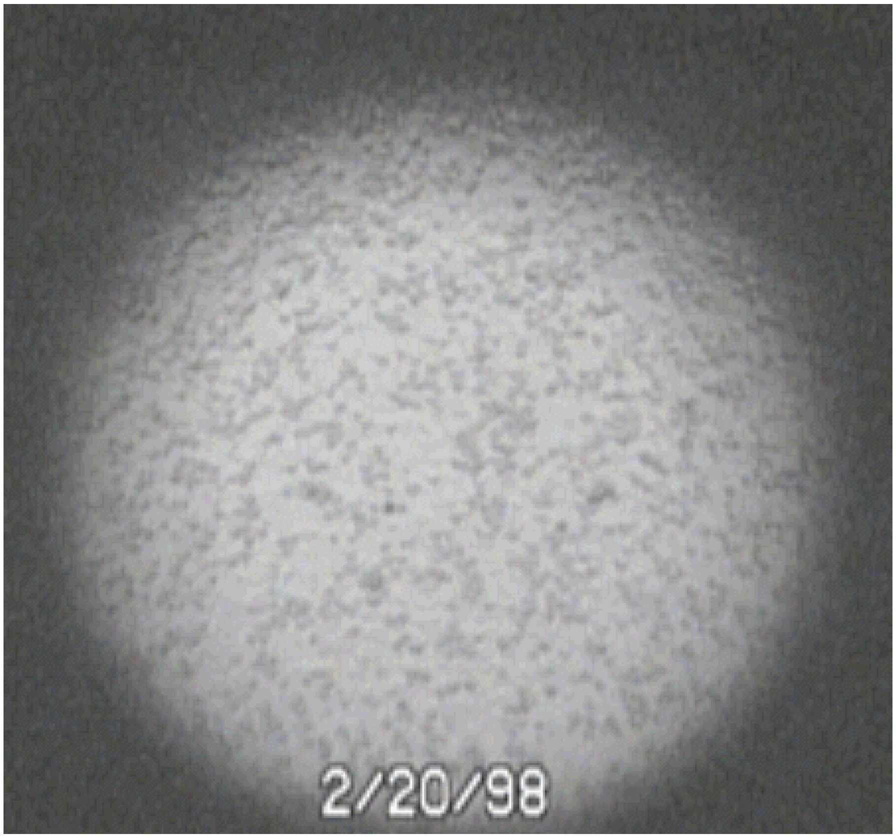

Figure 43 Microscope Image of 60,000 Seed Density (7003 pixels).

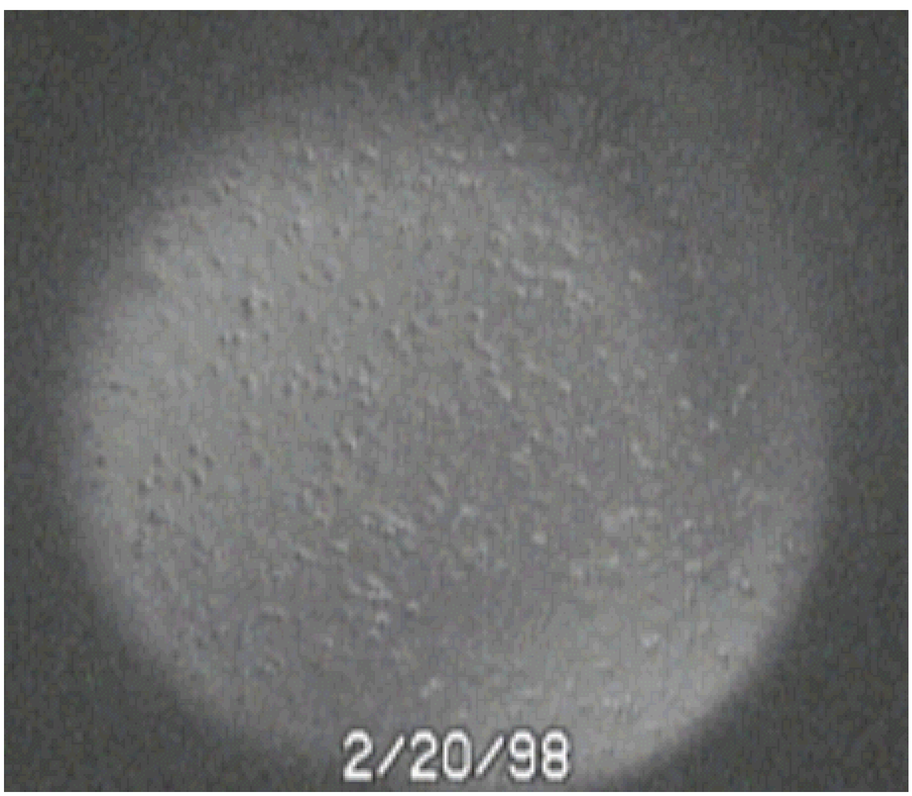

Figure 44 Microscope Image of 10,000 Seed Density (7507 pixels).

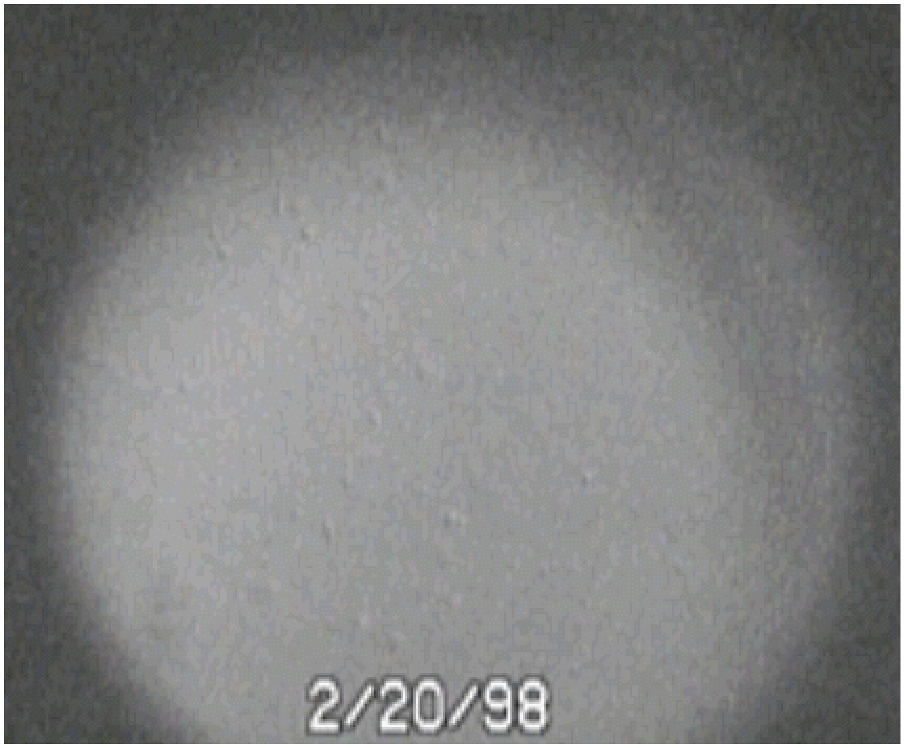

Figure 45 Microscope Image of 1,000 Seed Density (7674 pixels).

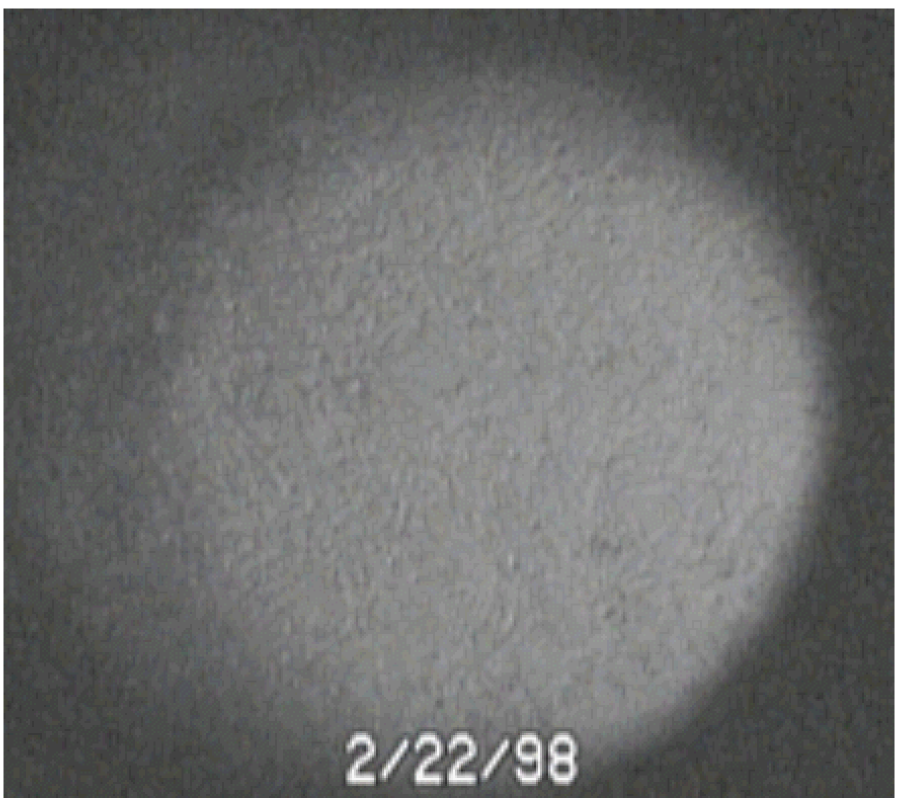

Figure 46 Microscope Image of 60,000 Seed Density (7289 pixels).

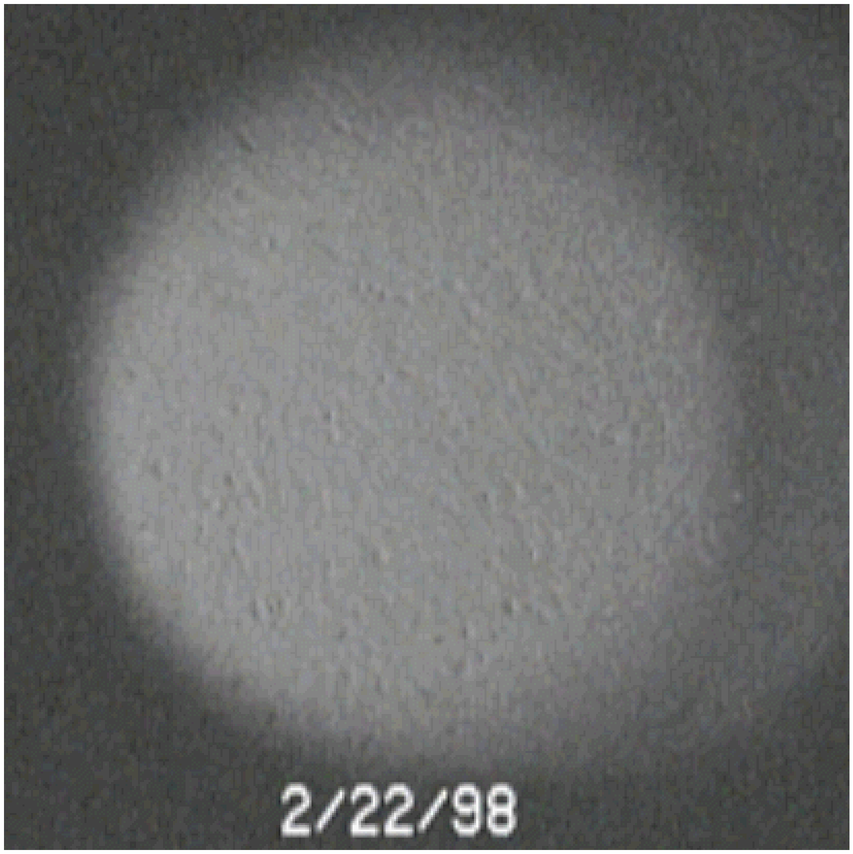

Figure 47 Microscope Image of 10,000 Seed Density (7249 pixels).

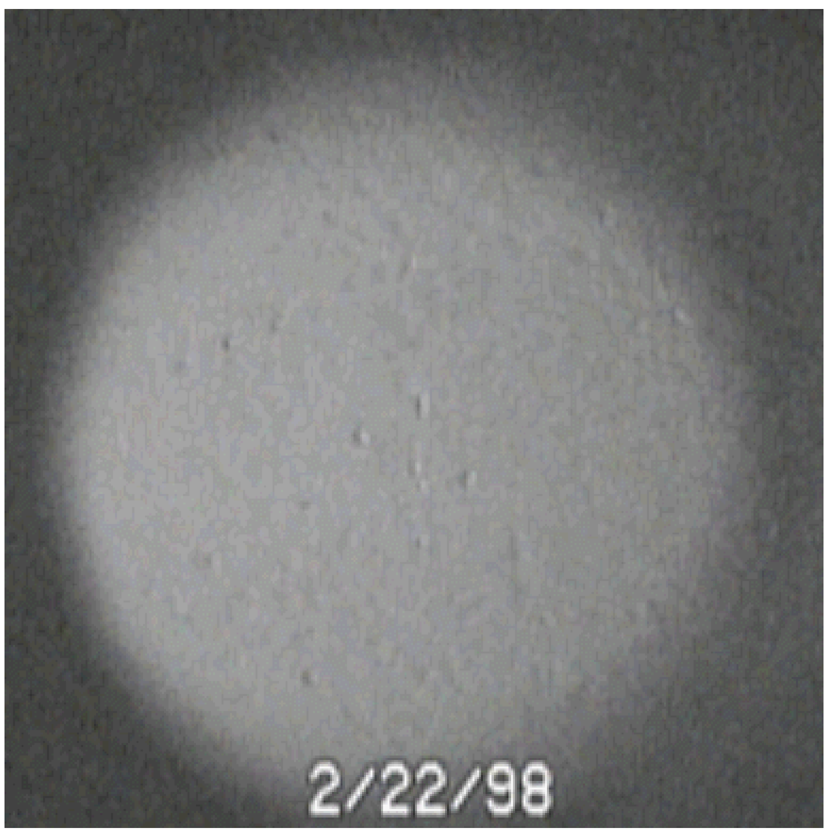

Figure 48 Microscope Image of 1,000 Seed Density (6930 pixels).

8. REFERENCES

[1] Fred P. Milanovich , http://www.llnl.gov/IPandC/home.shtml, Industrial Partnerships and Commercialization: Lawrence Livermore National Laboratory, Jan. 2, 1998.

[2] Sina Rabbany, Brian Donner, Frances Ligler, *Optical Immunosensors*, Critical Reviews in Biomedical Engineering, **1994**, 22(5/6), 307-346.

[3] Sina Rabbany, Brian Donner, Frances Ligler, Critical Reviews in Biomedical Engineering, **1994**, 22(5/6), 307-346.

[4] A.F. Collings, Frank Caruso, Reports on Progress in Physics, **1996**, 60 (11), 1397-1445.

[5] Sina Rabbany, Brian Donner, Frances Ligler, Critical Reviews in Biomedical Engineering, **1994**, 22(5/6), 307-346.

[6] A.F. Collings, Frank Caruso, Reports on Progress in Physics, **1996**, 60 (11), 1397-1445.

[7] R.D. Tilton, C.R. Robertson, A.P. Gast, Langmuir, **1991**,7, 2710.

[8] R.M. Gendreau, S. Winters, R.I. Leininger, D. Fink, C.R. Hassler, R.J. Jakobsen. Applied Spectroscopy, **1981**, 35, 355.

[9] Bruce Alberts, Dennis Bray, Julian Lewis, Martin Raff, Keith Roberts, James D. Watson, *Molecular Biology of the Cell 3rd ed*.; Garland, New York, 1994; pp. 899.

[10] Mary Burford, M.S. Thesis, *Material Process Monitoring with Optical Fiber Sensors*, Virginia Polytechnic Institute and State University, Aug. 1996.

[11] NIH Image Program, U.S. National Institutes of Health, http://rsb.info.gov/nih-image.

[12] S. Bradury, The Evolution of the Microscope; Pergamon Press: Oxford, 1967; pp. 31.

[13] S. Bradury, The Evolution of the Microscope; Pergamon Press: Oxford, 1967; pp. 315.

[14] Bruce Alberts, Dennis Bray, Julian Lewis, Martin Raff, Keith Roberts, James D. Watson, *Molecular Biology of the Cell 3rd ed*.; Garland, New York, 1994; pp. 147.

[15] Sina Rabbany, Brian Donner, Frances Ligler, Critical Reviews in Biomedical Engineering, **1994**, 22(5/6), 307-346.

[16] Sina Rabbany, Brian Donner, Frances Ligler, Critical Reviews in Biomedical Engineering, **1994**, 22(5/6), 307-346.

[17] John Greivenkamp Jr. in *Handbook of Optics 2nd ed*.; Michael Bass Ed. McGraw-Hill; New York, 1995; pp. 2.19.

[18] Lehninger, Nelson, and Cox *Principles of Biochemistry,* Worth, New York, 1993; Chapter 2.

[19] Bruce Alberts, Dennis Bray, Julian Lewis, Martin Raff, Keith Roberts, James D. Watson, *Molecular Biology of the Cell 3rd ed*.; Garland, New York, 1994; pp. 949.

[20] John Powers. *An Introduction to Fiber Optic Systems 2nd ed.*; pg. 167, Irwin, Chicago, 1997.

VITA

Douglas West was born on October 31, 1966 in Melbourne, Florida. After finishing high school in 1984, he joined the United States Air Force and served there until 1994. He was stationed at RAF Upper Heyford, United Kingdom where he attended Oxford Polytechnic Institute. He was transferred to New Mexico where he completed his Bachelor of Science degree at Eastern New Mexico University, majoring in Professional Chemistry with minors in Electronics and Mathematics.

In August of 1996 he enrolled in a Master of Science in Materials Science and Engineering Program at Virginia Polytechnic Institute and State University. Upon leaving Virginia Polytechnic Institute and State University he will be filling the position of Senior Quality Reliance Engineer for the Intel Corporation in Folsom, California. Awards include the Air Force Achievement Medal, Langley Aerospace Summer Scholars, Robert A. Welch Fellowship, and inclusion in "Who's Who in Science and Engineering."